

**DOKUZ EYLÜL UNIVERSITY**  
**GRADUATE SCHOOL OF NATURAL AND APPLIED SCIENCES**

**DETERMINATION OF DESIGN AND ANALYSIS  
PARAMETERS OF RAILS UNDER SYSTEM  
PRESSURE IN COMMON RAIL SYSTEMS**

by

**Ernur Güşav PİHAVA**

**October, 2014**

**İZMİR**

**DETERMINATION OF DESIGN AND ANALYSIS  
PARAMETERS OF RAILS UNDER SYSTEM  
PRESSURE IN COMMON RAIL SYSTEMS**

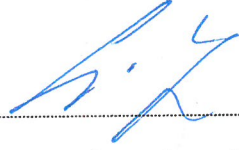
**A Thesis Submitted to the  
Graduate School of Natural and Applied Sciences of Dokuz Eylül University  
In Partial Fulfillment of the Requirements for the Degree of Master of Science  
in Mechanical Engineering, Mechanics Program**

**by  
Ernur Güşav PİHAVA**

**October, 2014  
İZMİR**

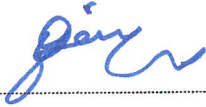
## M.Sc THESIS EXAMINATION RESULT FORM

We have read the thesis entitled “DETERMINATION OF DESIGN AND ANALYSIS PARAMETERS OF RAILS UNDER SYSTEM PRESSURE IN COMMON RAIL SYSTEMS” completed by ERNUR GÜŞAV PİHAVA under supervision of ASSOC.PROF.DR. ÇINAR EMİNE YENİ and we certify that in our opinion it is fully adequate, in scope and in quality, as a thesis for the degree of Master of Science.



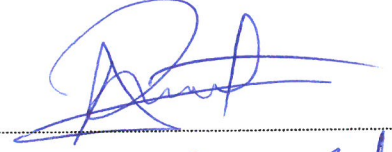
Assoc.Prof.Dr. Çınar Emine YENİ

Supervisor



Doç. Dr. Binnur Göres Kiral

(Jury Member)



Yrd. Doç. Dr. Aysun Baltacı

(Jury Member)



Prof. Dr. Ayşe OKUR

Director

Graduate School of Natural and Applied Sciences

## ACKNOWLEDGMENTS

I would like to thank Assoc. Prof. Dr. ınar Emine YENİ, Delphi Diesel Rail PE Manager Mehmet Onur TANSUĐ and Ernur KAZANCI, Core Engineering leader Samim ÖZER in the preparation and completion of my thesis. I would also like to thank Goşenay HATIK for her help and effort during my study.

Ernur Güşav PİHAVA



# **DETERMINATION OF DESIGN AND ANALYSIS PARAMETERS OF RAILS UNDER SYSTEM PRESSURE IN COMMON RAIL SYSTEMS**

## **ABSTRACT**

In this study, design and analysis parameters of rail tubes which are used in common rail diesel engines are evaluated. Autofrettage pressure and rail geometry are two of the most important parameters in the common rail system process. These parameters increase the strength-weight ratio and extend the rail's fatigue life. Autofrettage pressure generates a residual stress field in the cylinder wall. An analytical autofrettage procedure of a thick-walled cylinder is proposed with the aim of predicting the required autofrettage pressure for different rail geometries. A FEA validation is provided. The analytical solutions and the numerical results had a very good correlation and a similar overall stress distribution was obtained. The research work summarized in this thesis is a contribution towards a better understanding of an autofrettage phenomenon in the basis of rail geometry.

**Keywords:** Common rail injection system, autofrettage, equivalent von Misses stress, Zhu & Yang model

# ORTAK RAYLI ENJEKSİYON SİSTEMLERİNDE SİSTEM BASINCI ALTINDA RAY TASARIM VE ANALİZ PARAMETRELERİNİN BELİRLENMESİ

## ÖZ

Bu çalışmada ortak raylı enjeksiyon sistemlerinde çalışan ray parçasının tasarım ve analiz parametrelerinin hesaplamaları yapılmıştır. Otofretaj basıncı ve ray geometrisi en önemli tasarım parametrelerinden ikisidir. Bu parametreler malzemenin yorulma ömrünü etkilemektedir. Otofretaj basıncı malzeme üzerinde kalıntı gerilmeler oluşturur. Analitik olarak ofofretaj basıncı farklı ray geometrilerinde denenmiştir. Elde edilen sonuçlar FEA çıktıları ile desteklenmiştir. Analitik hesaplamalar ve FEA sonuçları arasında farklılık olsa da ortalama gerilme dağılımları benzerlik göstermektedir. Bu çalışmada ray geometrisini etkileyebilecek en önemli fenomenlerden biri olan ofofretaj prosesi incelenmiştir.

**Anahtar kelimeler:** Ortak raylı enjeksiyon sistemi, ofofretaj, eşdeğer von Mises gerilmesi, Zhu & Yang modeli

<b>CONTENTS .....</b>	<b>Page</b>
THESIS EXAMINATION RESULT FORM .....	ii
ACKNOWLEDGEMENTS .....	iii
ABSTRACT .....	iv
ÖZ .....	v
LIST OF FIGURES .....	ix
LIST OF TABLES .....	xi
<b>CHAPTER ONE - INTERNAL-COMBUSTION ENGINES.....</b>	<b>1</b>
1.1 Operating Principle and Classifications .....	1
1.2 Literature Survey .....	4
<b>CHAPTER TWO - DIESEL ENGINE BASICS.....</b>	<b>6</b>
2.1 The Diesel Engine .....	6
2.2 Diesel Engine Fundamentals .....	6
2.2.1 Direct-Injection Systems .....	7
2.2.2 Indirect-Injection Systems .....	8
2.2.3 Diesel Fuel Injection .....	9
2.2.3.1 Diesel- Engine Management .....	9
2.3 Diesel Injection System Operating Principle .....	11
2.3.1 Unit Injector & Unit Pump Systems .....	11
2.3.2 Common Rail Fuel Injection .....	12
2.3.2.1 System Design.....	13
2.3.2.2 Common Rail Systems .....	14
2.3.2.2.1 Fuel Tank .....	15
2.3.2.2.2 Fuel Supply Pump .....	15
2.3.2.2.3 Fuel Filter .....	15
2.3.2.2.4 Unit Pump .....	16
2.3.2.2.5 Rail .....	16

**CHAPTER THREE-RAIL COMPONENTS ..... 17**

3.1 High Pressure Valve (HPV) ..... 17

    3.1.1 Primary Functions ..... 17

    3.1.2 Secondary Functions ..... 17

3.2 High Pressure Sensor (HPS)..... 18

    3.2.1 Primary Functions ..... 18

    3.2.2 Secondary Functions ..... 18

3.3 Pressure Limiting Valve (PLV)..... 18

    3.3.1 Internal Implantation Variant ..... 18

    3.3.2 External Implantation Variant ..... 19

3.4 Rail Body ..... 19

    3.4.1 Material ..... 19

**CHAPTER FOUR-AUTOFRETTAGE PROCESS ..... 22**

4.1 General Description..... 22

4.2. Functional Description ..... 23

    4.2.1 Partially Autofrettaged Tube ..... 26

        4.2.1.1 Stress Distribution in Partially Autofrettaged Tube ..... 27

        4.2.1.2 Strain Distribution in Partially Autofrettaged Tube ..... 29

        4.2.1.3 Residual Stress Pattern ..... 30

        4.2.1.4 Optimum Radius of Elasto-Plastic Junction ..... 31

        4.2.4.5 Effect of Working Pressure ..... 33

**CHAPTER FIVE- NUMERICAL RESULTS AND SIMULATIONS..... 35**

5.1 Modelling ..... 35

5.2 Theoretical Calculation ..... 36



5.3 FEA Analysis .....	37
5.3.1 Meshing.....	37
5.3.2 Boundary Conditions and Loading .....	37
5.3.3 Analysis Settings.....	38
5.3.3.1 Results of First Analysis .....	39
5.3.3.2 Results of Second Analysis .....	40
5.3.4 Oblong Design .....	43
5.3.5 FEA Results for Micro- Hole Design .....	46
5.3.5.1 Oblong Design .....	46
5.3.5.2 Circular Design .....	47
<b>CHAPTER SIX – RESULTS .....</b>	<b>49</b>
6.1 Step 1 (Oblong –Circular Comparison without Micro – hole).....	50
6.2 Step 2 (Oblong –Circular Comparison with Micro – hole).....	51
<b>CHAPTER SEVEN- CONCLUSIONS .....</b>	<b>52</b>
<b>REFERENCES.....</b>	<b>53</b>
<b>APPENDICES .....</b>	<b>54</b>

## LIST OF FIGURES

Page

Figure 2.1 Diesel engine .....	6
Figure 2.2 Common types of direct-injection compression-ignition or diesel engine combustion systems .....	7
Figure 2.3 Two common types of small indirect-injection diesel engine combustion systems .....	8
Figure 2.4 Schematic of unit injector and unit pump system .....	12
Figure 2.5 Schematic of common rail system .....	13
Figure 2.6 Schematic of common rail system .....	14
Figure 3.1 High pressure valve types .....	17
Figure 3.2 High pressure sensor BOM (Bill of Materials) .....	18
Figure 3.3 Internal variant of PLV .....	18
Figure 3.4 External variant of PLV .....	19
Figure 4.1 Mechanical components of a common rail fuel injection system of a diesel engine .....	22
Figure 4.2 Stress and strain variation of autofrettage principle .....	24
Figure 4.3 Effect of an autofrettage principle .....	25
Figure 4.4 Cross-section of a partially autofrettaged thick-walled tube with static equilibrium of the control element .....	26
Figure 4.5 Distribution of applied principal stresses across the wall of a partially autofrettaged tube subjected to internal pressure .....	28
Figure 4.6 Residual stress pattern in autofrettaged cylinder .....	30
Figure 4.7 Variation of maximum von Mises stresses at different elasto-plastic radius .....	31
Figure 4.8 Variation of maximum von mises stresses at different elasto-plastic radii for different K values .....	32
Figure 4.9 Variation of maximum von Mises stresses at different autofrettage pressure .....	34
Figure 5.1 Section of tube .....	36
Figure 5.2 Schematic of meshing .....	37
Figure 5.3 Boundary conditions and loading .....	38

Figure 5.4 Path section .....	38
Figure 5.5 Schematic of pressure loading and stress distribution on cylinder .....	39
Figure 5.6 Stress distribution along cylinder thickness .....	40
Figure 5.7 Schematic of pressure loading and stress range on cylinder .....	40
Figure 5.8 Stress distribution along cylinder thickness .....	41
Figure 5.9 Comparison of stress distributions ( with autofrettage and without autofrettage ) .....	42
Figure 5.10 Comparison of elasto-plastic radius and minimum von Mises stresses	43
Figure 5.11 Oblong shape and circular shape .....	44
Figure 5.12 Meshing and path definition .....	44
Figure 5.13 Comparison of elasto-plastic radii and minimum von Mises stress .....	45
Figure 5.14 Micro-hole design and micro-hole meshing .....	46
Figure 5.15 Path for micro-hole design .....	47
Figure 5.16 Micro-hole design and micro-hole meshing .....	47
Figure 5.17 Path for micro-hole design .....	48
Figure 6.1 Overall comparison for compressive stress distribution .....	49
Figure 6.2 Overall comparison for tensile stress distribution .....	49

## LIST OF TABLES

Page

Table 1.1 Classification of the internal combustion engine .....	2
Table 3.1 Chemical composition of micro-alloy steel material .....	19
Table 3.2 Mechanical properties of micro-alloy steel at room temperature .....	20
Table 3.3 Chemical composition of micro-alloy steel .....	20
Table 3.4 Mechanical properties of rail material .....	21
Table 5.1 Mechanical properties of steel for FEA inputs .....	35
Table 5.2 Geometric features of cylinder .....	35
Table 5.3 Analytic results of rail tube .....	37
Table 5.4 Comparison of rail tube with autofrettage and without autofrettage .....	41
Table 5.5 “ $r_{opt}$ ” value for analytical and simulation results .....	43
Table 5.6 Overall results for circular and oblong design .....	45
Table 6.1 Overall results .....	50
Table 6.2 Comparison of FEA results and analytical calculation .....	51
Table 6.3 Difference in stress values .....	51

# CHAPTER ONE

## INTERNAL-COMBUSTION ENGINES

### 1.1 Operating Principle and Classifications

The internal combustion (IC) engine is the most frequently employed power source for motor vehicles. Internal-combustion engines generate power by converting chemical energy bound in the fuel into heat, and the heat thus converted into mechanical work. The conversion of chemical energy into heat is accomplished through combustion, while the subsequent conversion of this thermal energy into mechanical work is performed by allowing the heat energy to increase the pressure within a medium which then performs work as it expands (Bosch, 2007).

Liquids, which supply an increase in working pressure via a phase transformation (vaporization), or gases, whose working pressure can be increased through compression, are used as the working media. The fuels - largely hydrocarbons – require oxygen in order to burn; the required oxygen is usually supplied as a constituent of the intake air (Bosch, 2007).

If fuel combustion occurs in the cylinder itself, the process is called internal combustion. Continuous mechanical work is possible only in a cyclic process (turbo-engine) of heat absorption, expansion (production of work) and return of the working medium to its initial condition (cycle). If the working medium is altered as it absorbs heat, e.g. when a portion of its constituents serve as an oxidant, restoration of its initial condition is possible only through replacement (Bosch, 2007).

Table1.1 Classification of the internal combustion engine

INTERNAL COMBUSTION ENGINE							
		Open process			Closed process		
Type of Process		Internal Combustion			External combustion		
		Combustion gas ( working medium )			Combustion gas (working medium)		
					Phase transformation In working medium		
		No			Yes		
Type of Combustion		Cyclic Combustion		Continuous Combustion			
Type of Ignition		Auto Ignition	Continuous Combustion				
Type of Machine	Engine & Machine enclosing a working chamber	Diesel	Hybrid	Spark Ignition	Rohs	Striling	Steam
	Turbine & Gas Turbine	-	--	-	Gas	Hot Steam	Steam
Type of mixture		Heterogeneous		Homogenous		Heterogeneous	
		( In the combustion chamber )			In continuous flame		

The system in Table 1.1 is called an open cycle system, and is characterized by cyclic gas exchange (expulsion of the combustion gases and induction of the fresh charge). Internal combustion therefore always requires an open cycle (Bosch, 2007).

In external air/fuel mixture formation, the mixture is formed outside of the combustion chamber. In an external combustion system, the actual working medium remains chemically unchanged, and can thus be returned to its initial condition by suitable measures (cooling, condensation). This enables the use of a closed process. In addition to the main process characteristics (open/closed) and type of combustion (cyclic/continuous), the various combustion processes for internal combustion engines can also be defined according to their air/fuel mixture formation and ignition arrangements (Bosch, 2007).

In this type of mixture formation in external combustion systems, a largely homogenous air/fuel mixture is present when combustion is initiated, so it is also referred to as homogenous mixture formation (Bosch, 2007).

In internal air/fuel mixture formation, combustion chamber directly introduces the fuel. The later the internal mixture formation occurs, the more heterogeneous the air/fuel mixture will be at the time combustion is initiated. Internal mixture formation is therefore also called heterogeneous mixture formation. Externally supplied ignition designs rely on an electric spark or a glow plug to initiate combustion. In auto-ignition, the mixture ignites as it warms to or beyond its ignition temperature during the compression, or when fuel is injected into air whose boundary conditions permit evaporation and ignition (Bosch, 2007).

## 1.2 Literature Survey

Amin et al. (2013) have investigated the optimum design of autofrettaged thick walled cylinders by observing the flow stress distribution along the cylinders. They have determined that the stress distribution remains the same for the same  $k$  values. Comparison with Zhu & Yang's model has been also carried out to determine the optimum elasto-plastic radius,  $r_{opt}$  and optimum autofrettage pressure,  $p_{opt}$ . They have used the equivalent von Mises stress as the yield criterion. They have observed that the percentage of reduction of maximum von Mises stress increases as value of  $k$  and the working pressure increases. The maximum von Mises stress is minimum for lower working pressure at same value of  $k$  and autofrettage pressure. They have observed that the autofrettage process never starts if the autofrettage pressure does not exceed the working pressure. They have also observed that the two limits of the autofrettage pressure  $P_{y1}$  and  $P_{y2}$  are not appropriate. The effect of the loading stages on autofrettage process is also investigated. As long as the pressures in the first and last stages remain constant, there is no effect of loading stages on autofrettage process; no matter how many stages prevail between these two pressures.

Basara (2007) has evaluated the high pressure components of fuel injection systems, especially those having complex geometries, by using Speckle Interferometry. Experimental testing indicated that speckle interferometry, compared with conventional measuring techniques, offers great potential for that purpose. Full-field measurements over the outer surface of the component using speckle interferometry allowed for the detection of strain gradients. By analysis of the strain gradients measured on the outer surface, he has evaluated the spreading of plastic deformation inside a component having a complex geometry (e.g. autofrettage in a bend of a fuel line). He has also investigated the influence of the pressure holding time on stress-strain generation during the autofrettage process, where the components in an industrial series production are held at the autofrettage pressure for several seconds. In doing so, he has assumed that a required stress-strain pattern was generated.



The experimental part of his work indicated that fuel lines should be autofrettaged at some higher pressure for a short period of time instead of keeping them for a longer period at the pressure determined by the analytical calculation. In this way, a desirable stress-strain state can be generated during the time required to maintain a profitable series production ( $t_s \text{ holding} < 10$ ). The results of his investigation also showed that speckle interferometry offers great potential for localization of cracks in a fuel line wall by analysis of the strain maps measured on the outer surface of the fuel line.

Wahi et. al. (2011) have investigated the effect of optimum autofrettage on pressure limits of thick-walled cylinders. In their optimal design of thick-walled cylinders, they aimed to achieve two objectives: increasing its strength-weight ratio and extending its fatigue life. They have proposed an analytical autofrettage procedure of a thick-walled cylinder, with the aim of predicting the required autofrettage pressure for various levels of allowable pressure and hence achieving maximum fatigue life. They have provided a Finite Element Method (FEM) validation. Their results reveal three scenarios in the design of thick-walled cylinders. For maximum load carrying capacity, non-autofrettage is suitable when, in service, the whole wall thickness will be yielded. Full autofrettage is suitable when, during subsequent operation, yielding is limited at the inner surface. Optimum autofrettage of the cylinder is suitable if a minimum equivalent stress and maximum fatigue life are to be achieved. Their analytical solutions compared satisfactorily to the numerical results where a very good correlation in form and magnitude was obtained.

## **CHAPTER TWO**

### **DIESEL ENGINE BASICS**

#### **2.1 The Diesel Engine**

The diesel engine, Figure 2.1, invented in the late 19th century by Dr. Rudolf Diesel, is the most energy efficient power plant among all types of internal combustion engines known today. This high efficiency translates to good fuel economy and low greenhouse gas emissions. Other diesel features that have not been matched by competing energy conversion machines include durability, reliability, and fuel safety. The downsides of diesels include noise, low specific power output, NO<sub>x</sub> and PM emissions, and high cost.



Figure 2.1 Diesel engine

#### **2.2 Diesel Engine Fundamentals**

The diesel engine is a compression-ignition internal combustion heat engine which can be operated in both four- and two-stroke cycles. The combustion process can be theoretically modeled by applying thermodynamic laws of mass and energy conservation to the processes in the engine cylinder. Basic design and performance parameters in diesel engines include the compression ratio, swept volume, clearance volume, a number of scavenging characteristics in two-stroke engines, power output,

indicated power, mechanical efficiency, indicated mean effective pressure, brake mean effective pressure, specific fuel consumption, and more (Magdi & Hannu, 2011).

Diesel engines are divided into two basic categories according to their combustion chamber designs: (1) *direct-injection* (DI) *engines*, Figure 2.2, which have a single open combustion chamber into which fuel is injected directly; (2) *indirect – injection* (IDI) *engines*, Figure 2.3, where the chamber is divided into two regions and the fuel is injected into the ‘pre-chamber’ which is connected to the main chamber (situated above the piston crown) via a nozzle, or one or more orifices. IDI engine designs are only used in the smaller engine sizes. Within each category there are several different chamber geometries, air-flow, and, fuel–injection arrangements (Heywood, 1988).

### 2.2.1 Direct-Injection Systems

In the larger–size engines, where mixing rate requirements are least stringent, quiescent direct-injection systems shown in Figure 2.2a are used. The momentum and energy of the injected fuel jets are sufficient to achieve adequate fuel distribution and rates of mixing with air. Additional organized air motion is not required. The combustion chamber shape is usually a shallow bowl in the crown of the piston, and a central multi-hole injector is used.

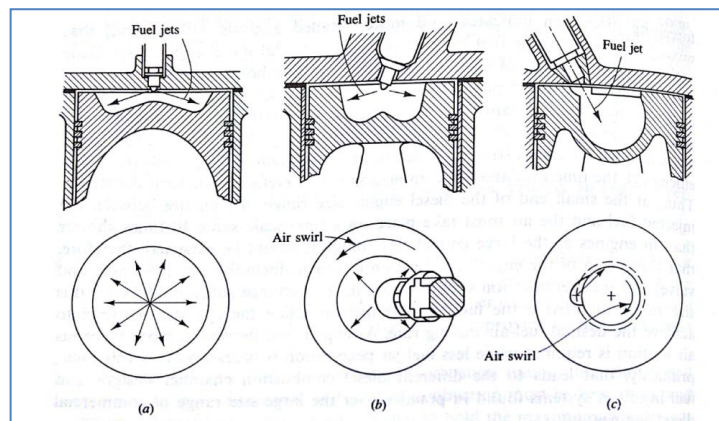


Figure 2.2 Common types of direct-injection compression-ignition or diesel engine combustion systems (a) Quiescent chamber with multihole nozzle typical of larger engines (b) Bowl-in-piston chamber with swirl and multihole nozzle; (c) Bowl-in-piston chamber with swirl and single-hole-nozzle.

As the engine size decreases, increasing amounts of air swirl are used to achieve faster fuel-air mixing rates. Air swirl is generated by suitable design of the inlet port; the swirl rate can be increased as the piston approaches chamber by forcing the air toward the cylinder axis, into a bowl-in-piston type of combustion chamber (Heywood, 1988).

Figure 2.2a and Figure 2.2c shows the two types of DI engines with swirl in common use. Figure 2.2b shows a DI engine with swirl, with a centrally located multi-hole injector nozzle. Here the design goal is to hold the amount of liquid fuel which impinges on the piston cup walls to a minimum. Figure 2.2c shows the ‘M System’ with its single-hole-fuel-injection nozzle, oriented so that most of the fuel is deposited on the piston bowl walls. These two types of designs are used in medium size (10- to 15-cm bore) diesels and, with increased swirl, in small-size (8-to 10-cm bore) diesels (Heywood, 1988).

### 2.2.2 Indirect-Injection Systems

Inlet generated air swirl, despite amplification in the piston cup, has not provided sufficiently high fuel-air mixing rates for small high-speed diesels such as those used in automobiles. Indirect-injection or divided-chamber engine systems have been used instead, where the vigorous charge motion required during fuel injection is generated during the compression stroke.

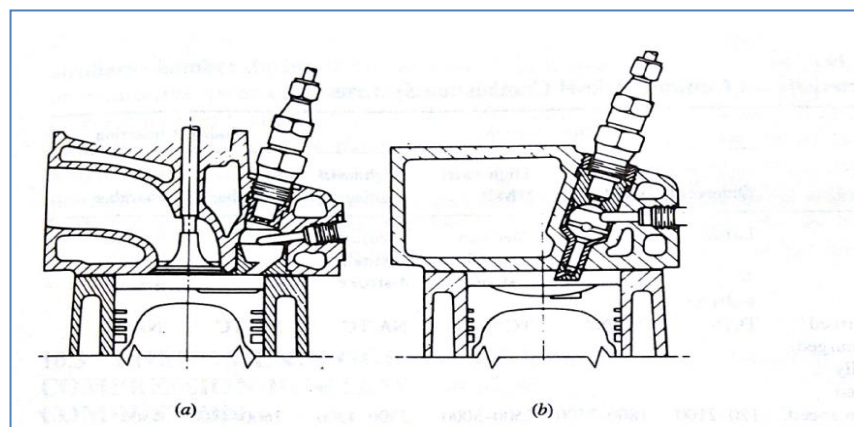


Figure 2.3 Two common types of small indirect-injection diesel engine combustion systems: (a) Swirl pre-chamber; (b) turbulent pre-chamber

Two broad classes of IDI systems can be defined: (1) swirl chamber systems and (2) pre-chamber systems, as illustrated in Figure 2.3a and Figure 2.3b respectively. During compression, air is forced from the main chamber above the piston into the auxiliary chamber, through the nozzle or orifice. Thus toward the end of the compression, a vigorous flow in the auxiliary chamber is set up; in swirl chamber systems the connecting passage and chamber are shaped so that this flow within the auxiliary chamber rotates rapidly (Heywood, 1988).

### ***2.2.3 Diesel Fuel Injection***

In the diesel combustion process, the fuel is always injected directly into the combustion chamber at a nozzle pressure ranging from 200 to  $> 2,000$  bar. Depending on the combustion process, fuel is injected into a pre-chamber in indirect injection engines (at a relatively low pressure of  $< 350$  bar). In the meantime, direct injection has become the most common process, in which fuel is injected (at high pressure up to  $> 2,000$  bar); into the non-divided combustion chamber (Bosch, 2007).

#### ***2.2.3.1 Diesel- Engine Management***

***2.2.3.1.1 Requirements.*** The power output  $P$  from a diesel engine is determined by the available clutch torque and the engine speed. The clutch torque is produced from the torque generated by the combustion process, reduced by the friction torque and the charge-cycle losses, and the torque required for operating the auxiliary systems driven directly by the engine. The combustion torque is generated in the power cycle and is determined by the following variables if the excess is sufficient.

- The supplied fuel mass
- The start of combustion determined by the start of injection
- The start of injection
- The injection / combustion process

In addition , the maximum speed-dependent torque is limited by

- Smoke emissions
- The cylinder pressure
- The temperature load of different components
- The mechanical load of the complete drive train

Primary function of engine management:

The primary function of engine management is to adjust the torque generated by the engine or, in some applications, to adjust a specific engine speed within the permitted operating range (e.g. idling) (Bosch, 2007).

In a diesel engine, exhaust–gas treatment and noise suppression are performed to a great extent inside the engine, i.e. by controlling the combustion process. This, in turn, is performed by engine management by changing the following variables.

- Cylinder charge
- Tempering of the cylinder charge during the induction stroke
- Composition of the cylinder charge (exhaust – gas recirculation)
- Charge motion ( intake swirl)
- Start of injection
- Injection pressure
- Rate-of-discharge curve control (e.g. pilot injection, divided fuel injection etc.)

Until the 1980s fuel injection in vehicle engines, i.e. injected fuel quantity and start of ignition, was governed exclusively by mechanical means. Here, the injected fuel quantity is varied via a helix on the plunger or via sleeves as a function of load and speed. In the case of mechanical injection, the start of injection/delivery is adjusted by flyweight governors (speed dependent), or hydraulically by pressure control as a function of speed and load. This is discussed in more detail in sections headed ‘‘In-line injection pump’’ and ‘‘distributor injection pump’’ (Bosch, 2007).

Emission-control legislation calls for highly precise control of the injected fuel quantity and start of injection as a function of variables such as temperature, speed, load, height, etc. This can only be provided effectively by electronic control. This form of control has become widespread not just in automotive field. This is the only form of control that permits continuous monitoring of the emission-related function of the fuel injection system. Legislation also requires on-board diagnosis in some applications (Bosch, 2007).

Control of injected fuel quantity and start of injection is performed in EDC (Electronic Diesel Control) systems by means of low or high-pressure solenoid valves or other electrical actuators. Control on the rate of discharge, i.e. the quantity provided per crankshaft degree, can be performed indirectly by means of a servo valve and needle lift-control (Bosch, 2007).

## **2.3 Diesel Injection System Operating Principle**

### ***2.3.1 Unit Injector & Unit Pump Systems***

In unit injector and unit pump injection systems, a separate pump serves each engine cylinder. The unit injector system, figure 2.4 has the capability to develop the highest injection pressure among all types of injection systems. Advanced, electronically controlled unit injector systems have also the capability for multiple injections and rate shaping.

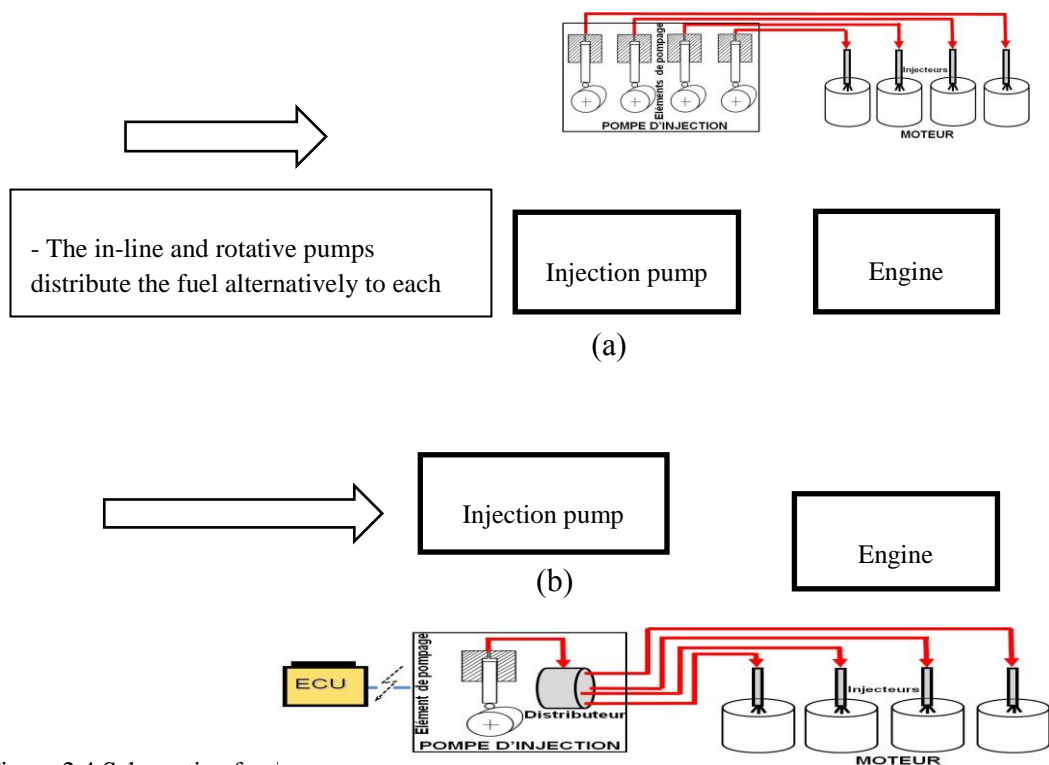


Figure 2.4 Schematic of unit injector and unit pump system: (a) in-line pumps; (b) rotative pumps.

### 2.3.2 Common Rail Fuel Injection

In the common rail system, fuel is distributed to the injectors from a high pressure accumulator, called the rail. The rail is fed by a high pressure fuel pump. The pressure in the rail, as well as the start and end of the injection in each cylinder are electronically controlled. Advantages of the common rail system include flexibility in controlling both the injection timing and injection rate. Stable pilot injections which can be delivered by the common rail have proven to lower the engine noise and the  $\text{NO}_x$  emissions.



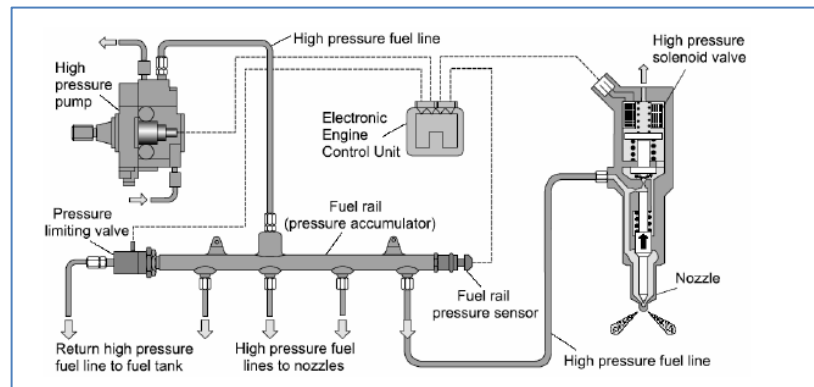


Figure 2.5 Schematic of common rail system.

Common-rail (accumulator) fuel-injection systems, figure 2.5 make it possible to integrate the fuel injection systems together with a number of its extended functions in the diesel engine, and thus increase the degree of freedom available for defining the combustion process.

The common rail system's principal feature is that injection pressure is independent of engine speed and injected fuel quantity. This is only the case with the common rail systems and not with all the cam-driven systems described previously (Bosch, 2007).

### 2.3.2.1 System Design

The functions of pressure generation and fuel injection are separated by an accumulator volume. This volume, which is essential to the correct operation of the system, is made up of the common fuel rail, the fuel lines and the injectors themselves (Bosch, 2007).

The system is generated by a high pressure plunger pump. This pump is partly designed as an in-line –injection pump for commercial vehicles and otherwise as a radial-piston-pump. The pump operates at low maximum torques and thus substantially reduces drive–power requirements in high–pressure pumps for passenger cars; the desired rail pressure is regulated by a pressure–control valve mounted on the high–pressure side of the pump or the rail (Bosch, 2007).

High pressure pumps for commercial vehicles and the second generation for passenger cars have an injected-fuel quantity control system on the intake side. This reduces the temperature of the fuel within the system. The system pressure generated by the high pressure pump and regulated by a pressure-control circuit is applied to the injector. This injector serves as the core of this concept by ensuring correct fuel delivery into the combustion chamber (Bosch, 2007).

At a precisely defined instant the control unit transmits an activation signal to the injector solenoid to initiate fuel delivery. The injected fuel quantity is defined by the injector opening time and the system pressure. The control unit, sensors and most of the other system are basically the same as in other time-controlled single cylinder pump systems (Bosch, 2007).

#### 2.3.2.2 Common Rail Systems

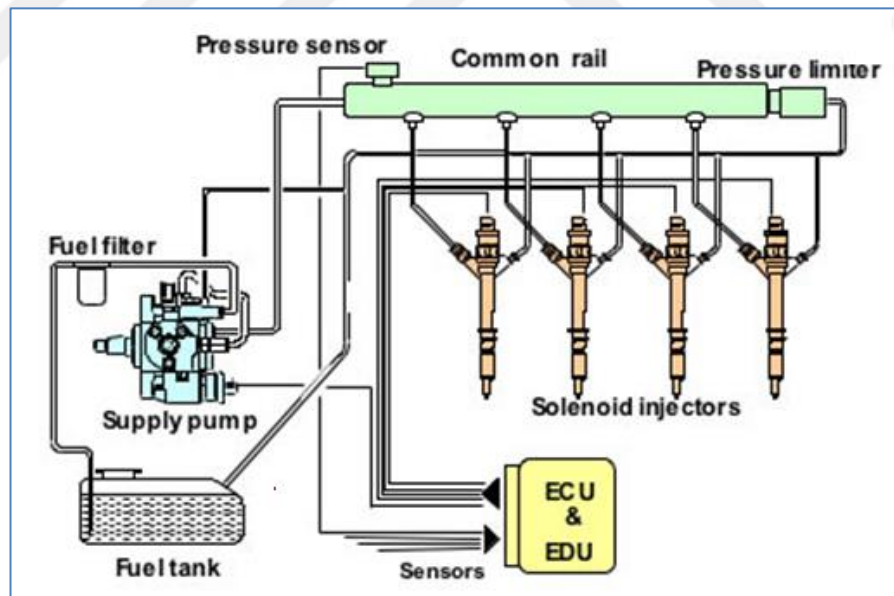


Figure 2.6 Schematic of common rail system

*2.3.2.2.1 Fuel Tank.* The fuel tank stores the fuel. It must be corrosion-resistant and leak-proof to pressures which are double the operating pressure, but at least to gage pressure of 0.3 bars. Gage pressure that occurs must escape automatically through suitable openings of safety valves. When the vehicle is cornering, is at an inclined position, or is subject to jolts or impacts, no fuel is permitted to emerge from the filler plug or the pressure-compensation devices (Delphi product training, 2013).

*2.3.2.2.2 Fuel-Supply Pump.* The function of the fuel supply pump in the low-pressure stage (pre-supply pump) is to supply the high pressure components with sufficient fuel (Delphi product training, 2013).

- In operating stage
- With a low level of noise
- At the required pressure and
- Over the entire service life of vehicle

As shown in figure 2.6 different types are used, depending on the field application,

- Electric fuel pump
- Gear pump
- Vane type supply pump

*2.3.2.2.3 Fuel Filter.* The function of the fuel filter is to prevent the fuel from being contaminated by particulates and to ensure a minimum level of fuel purity upstream of components subject to wear. The right choice of filter is dependent on the fuel injection system used and on the operating condition.

The preliminary filter is usually a strainer with a mesh size of 300  $\mu\text{m}$  and is used in addition to the actual fuel filter.

2.3.2.2.4 *Unit Pump*. The unit pump presented in this article is simply composed of a pumping element assembled in a compact pump hydraulic head. Roller tappet assembly is the part of the pump which transfers the rotational movement of the cam shaft to the linear movement of the pumping element and is lubricated by the engine oil (Delphi product training, 2013).

2.3.2.2.5 *Rail*. Rail is mid-fuel reservoir of the fuel injection equipment and it is needed for the fuel distribution. For the above purpose, basically a rail is a thick tube with damping orifices in order to prevent big pressure drops during injections and keep feeding fuel injectors. These orifices damp the pressure waves due to injection and avoid too much interaction between multiple injections, Figure 2.6 (Delphi product training, 2013).

## CHAPTER THREE

### RAIL COMPONENTS

#### 3.1 High Pressure Valve (HPV)

High Pressure valve has two main functions at common rail systems.

##### 3.1.1 Primary Functions

- Lower the pressure in the high pressure circuit by discharging fuel,
- Maintain a minimum pressure in the rail to start and run the engine in case of an open circuit of the actuator (HPV normally closed),
- Purge the rail when the engine is switched off by discharging pressurized mixture of “Air + fuel” (HPV normally open).

##### 3.1.2 Secondary Functions

Control the high pressure in the rail in case of:

- An open circuit on the electrical circuit of the Inlet Metering Valve (IMV)
- On systems without any Inlet Metering Valve (IMV)
- A fault on the High Pressure Sensor (HPS)
- Limit the pressure in case of overpressure in the high pressure circuit

Regarding the system design, two kinds of HPV can be used, Figure 3.1.

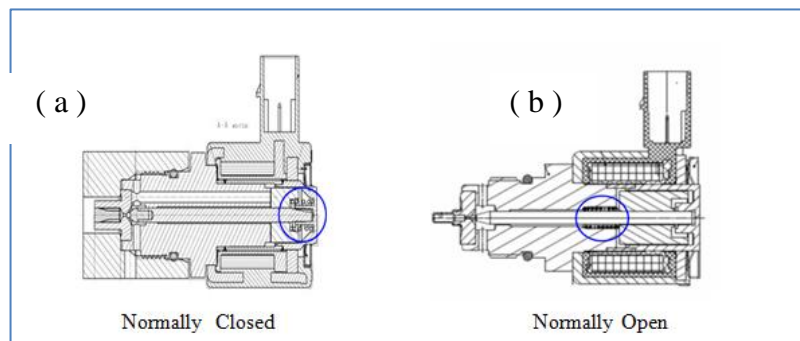


Figure 3.1 a ) Normally closed high Pressure valve, b) Normally open high pressure valve.

## 3.2 High Pressure Sensor (HPS)

### 3.2.1 Primary Functions

As shown in figure 3.2 providing fuel pressure feedback to the  $\mu$ -processor of the controller (Electronic control unit ), figure 3.2 in order to adjust the "fuel quantity" and "pulse timing" managed by the pressure control "closed loop" strategy (Delphi product Training 2013).

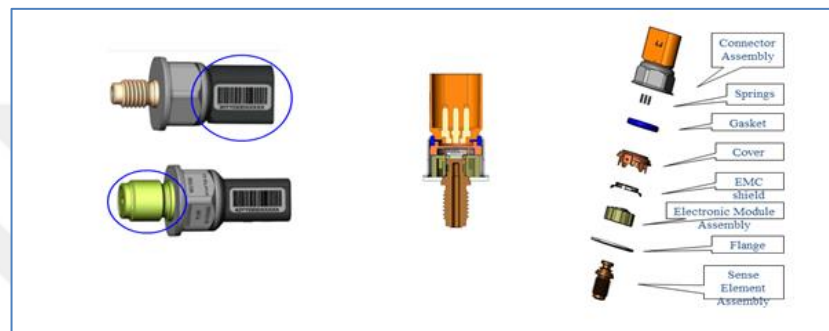


Figure 3.2 High Pressure Sensor BOM (Bill of Materials)

### 3.2.2 Secondary Functions

Detection of internal failure such as a broken wire bond.

## 3.3 Pressure Limiting Valve (PLV)

### 3.3.1 Internal Implantation Variant

- Installed internally in the rail body, figure 3.3
- Biting edge interface for high pressure sensor sealing as HP sensor.

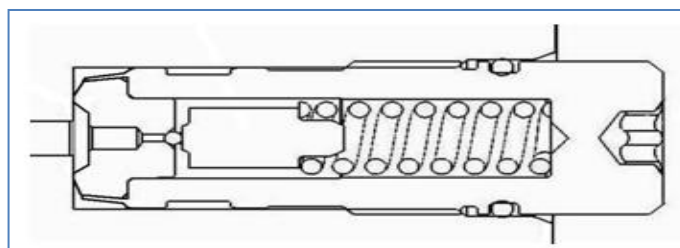


Figure 3.3 Internal variant of PLV

### 3.3.2 External Implantation Variant

- Installed externally to the rail body, figure 3.4
- Biting edge interface for high pressure sealing as HPV



Figure 3.4 External variant of PLV.

## 3.4 Rail Body

### 3.4.1 Material

Rail body material must resist high pressure applications. Steel (suitable for forging or welding) is used at production process.

For the welded rail, the material is exclusively supplied as ready-processed components. High pressure accumulators are manufactured by hot rolling or cold drawing. The material has high pressure resistance and durability. Tables 3.1 and 3.2 show the chemicals composition and mechanical properties of steel material.

Table 3.1 Chemical composition of micro-alloy steel material

	C	Si	Mn	P	S	N	Cr	Cu	Mo	Ni	Nb	Ti	V
min		0.1	1.00										
max	0.22	0.6	1.70	0.03	0.03	0.02	0.3	0.25	0.1	1.00	0.05	0.2	0.20

Table 3.2 Mechanical properties of micro-alloy steel at room temperature

<b>Delivered State</b>		<b>Yield Strength</b>	<b>Tensile Strength</b>	<b>Strain</b>
		N/mm <sup>2</sup>		%
Cold drawn / hard (PPCD)		min.780	min.850	min.12
Defined/heat treated (PPAH)		min.850	min.980	min.15

For forged rail, micro-alloyed steel suitable for hot forging or cold forming and capable of producing of 1000 MPa tensile strength is used. Material is delivered as rolled and soft annealed to improve cold shearing. Tables 3.3 and 3.4 show the chemical composition and mechanical properties of this material (Delphi Material Specification, 2011).

Table 3.3 Chemical composition of micro-alloy steel

<b>Element</b>	<b>%</b>
Carbon	0.35-0.45
Silicon	0.5 max
Manganese	1.3-1.7
Sulphur	0.06-0.08
Phosphorus	0.025 max
Vanadium	0.08-0.2
Lead	0.15-0.2
Cromium	0.3 max
Molybdenum	0.08 max
Nitrogen	0.01-0.02



Table 3.4 Mechanical properties of rail body

<b>PROPERTY</b>	<b>UNIT</b>	<b>After normalizing( see note )</b>
Tensile Strength (according EN 10002-1)	MPa	900-1100
Elongation on $5.65\sqrt{S_0}$	%	8 min.
Yield Strength $R_{p0.2}$	MPa	650 min.
Hardness (According ISO 6506-1)	HBW	270-330

A special treatment (Autofrettage process) is used to plastify the critical area at the rail body. Thus the rail's robustness and reliability could be improved. However welded body material's mechanical properties are better than the forged material, and the forged material has better autofrettage characteristics. Thus forged rail will be examined at this study. Autofrettage parameter and effects will be studied in the next pages.

## CHAPTER FOUR

### AUTOFRETTAGE PROCESS

#### 4.1 General Description

The fuel injection systems of diesel engines require significantly higher operating pressures when compared to the systems of gasoline engines. This is due to the higher air compression ratio of a diesel engine, to the higher viscosity of a diesel fuel, and to the difference of the hydrodynamic behaviour and the difference in the working principle of a diesel engine. The design and development of mechanical components for such systems are therefore more complex (Basara, 2007).

A characteristic feature of any high pressure process is exhibiting at absolutely artificial environments far beyond those existing in nature. The operating pressures in such processes are in the range from 100 to 10000 bar and can be of a static or fluctuating nature. High pressure components are required to maintain these conditions for long lifetime. Owing to the extremely high pressures, the material of component is usually stressed even statically up to its strength limit.

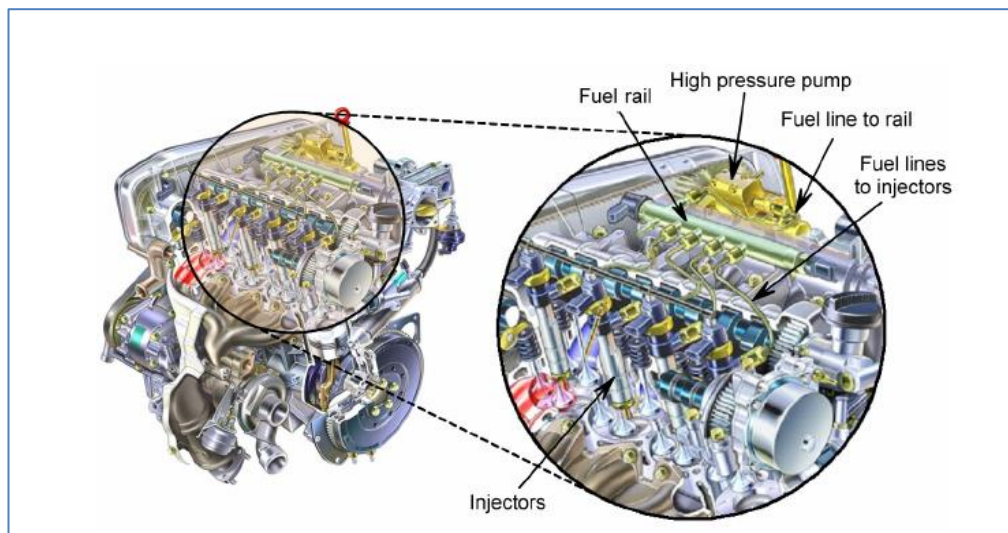


Figure 4.1 Mechanical components of a common rail fuel injection system of a diesel engine.

Mechanical components of the fuel injection system, Figure 4.1 are stressed with extremely high fluctuating pressure amplitudes for a long time. (More than 1000 injections per minute). This permanent change between a higher and a lower pressure causes a cyclic stress in the material, which leads to fatigue of the material until mechanical failure of the component occurs. The fatigue strength of the component exposed to the fluctuating load is generally lower than the yield strength and it decreases as the number of loading cycles increases. Therefore, it presents a major challenge to design and develop the components that have to be suitable for safe operation under such extremely fluctuating pressure amplitudes for a long time. An autofrettage process is a manufacturing procedure wherein the component is subjected to a static internal pressure far beyond the intended operating pressure in order to induce a partial yield of the component. After a short period of time, the component is unloaded and the required permanent plastic deformation is reached. The plastic deformation is accompanied by the generation of residual stresses in the component (Basara, 2007).

The objective of the autofrettage process is to obtain a favourable residual stress pattern in a manufacturing process which brings beneficial effects under the operating conditions. By application of the autofrettage process, the static loading capability of components can be increased due to the residual stress pattern. This pattern reduces crack initiation, retards the fatigue crack growth rate and consequently increases the fatigue limit of the component (Basara,2007).

## **4.2 Functional Description**

Autofrettage is a process in which the part is subjected to a certain amount of a pre-internal pressure so that its walls become partially plastic. The pressure is then released and the residual stress lead to decrease in the maximum von- Mises stress in the working loading stage. This means an increase in the pressure capacity of the part.

In autofrettage the aim is to increase the fatigue reliability performances of the rail body. The autofrettage consists to install in the rail body material some residual compressive stresses by applying a fluid pressure in the rail cavity.

When a component is pressurized by an autofrettage pressure, which is much higher than the working pressure and is dependent on the material used, hardness, and the geometry of component, the inner boring will be formed plastically and the deeper areas of the component of the wall will be formed elastically.

After relieving the autofrettage pressure from the component, the elastically formed areas try to return to their original state while the plastically formed areas prevent this process. Therefore, internal stresses are created in a huge part of the wall thickness which tries to work against the stresses that arise from normal working pressure. Under working pressure the stresses inside the component do not move between zero and maximum value any more, but start in the pressure area below zero and end at a much lower maximum value (White Paper Autofrettage, 2013).

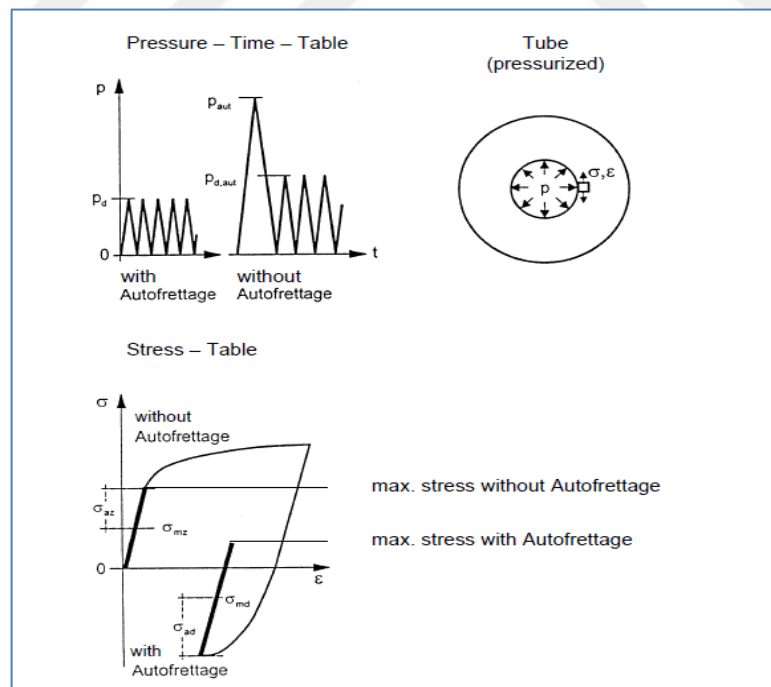


Figure 4.2 Stress and strain variation of autofrettage principle.

As can be seen from Figure 4.2 the resulting working loads (e.g. in the pipe) can be reduced considerably. A working pressure which would have led to a failure of the component prior to autofrettage now can be used endlessly - at least for a considerably longer time without failure. The permanent deformation of a thick-walled tube through this internal cold working process has been known since the time when Austrian general Uchatius discovered the principle of strengthening the bronze barrels for artillery guns. The earliest deliberate application of the autofrettage principle was at the beginning of the twentieth century in the French gun-barrel industry, but also in other industries such as the chemical, nuclear, automotive, artificial diamond industry, and most recently even in the food industry (Basara, 2007).

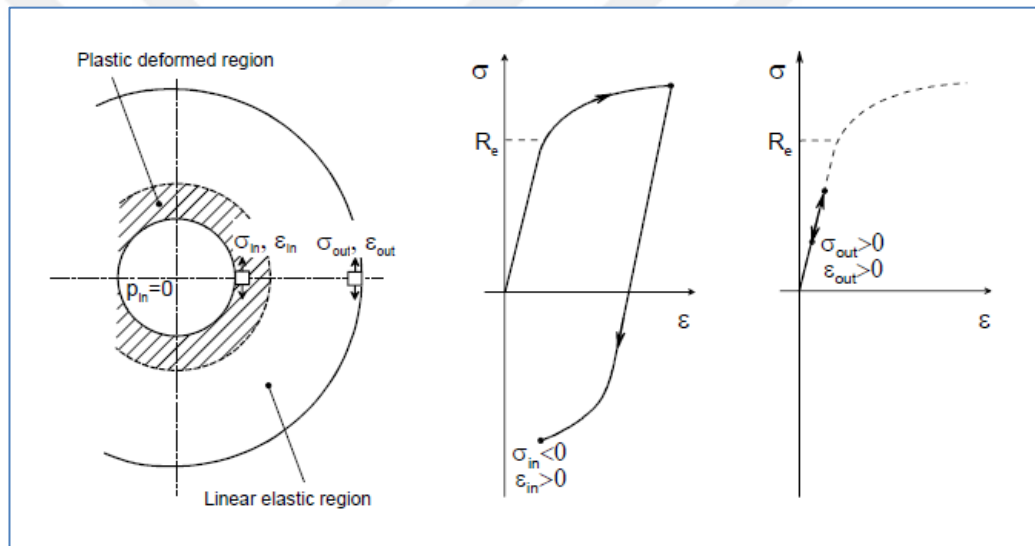


Figure 4.3 Effect of an autofrettage principle.

For the purpose of stress-strain analysis, an elastic-plastic thick-walled tube, Figure 4.3, subjected to an internal pressure ( $p_{in}$ ) is considered. Also in this case a two-dimensional stress state acting at the control element can be described by a differential Equation 4.1. Solutions of the equations for two different cases of an elastic-plastic thick walled tube (partially autofrettaged) is outlined here.

$$\sigma_{\varphi} - \sigma_r - r \cdot \frac{d\sigma_r}{dr} = 0 \quad (4.1)$$

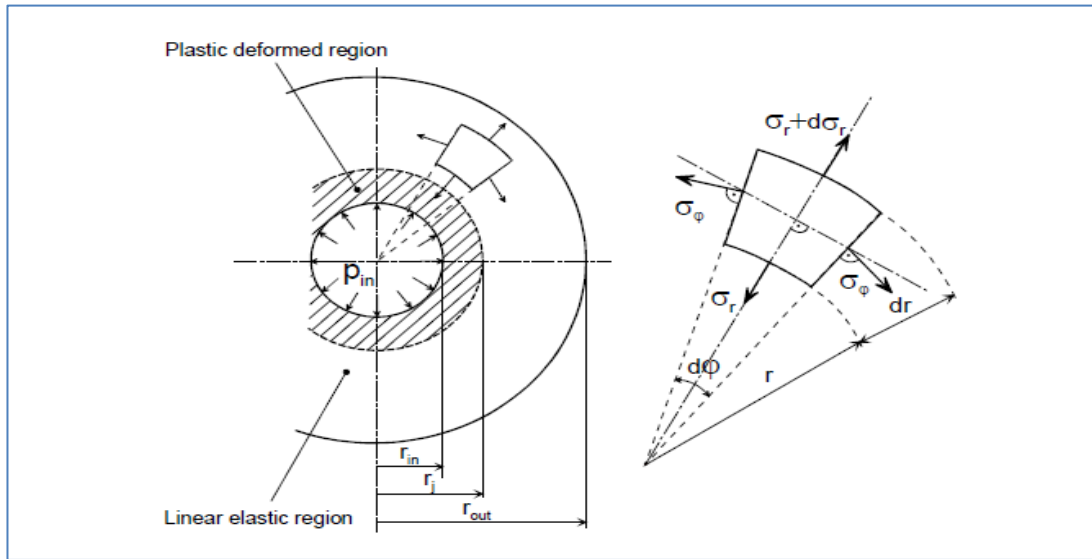


Figure 4.4 Cross-section of a partially autofrettaged thick-walled tube with static equilibrium of the control element.

#### 4.2.1 Partially Autofrettaged Tube

In the case of a partially autofrettaged tube Figure 4.3, it is assumed that the tube yields up to a certain point defined by the radius  $r_j$  and beyond that point it remains linearly elastic. The distance  $r_j$  is the distance from the tube axis to boundary of the plastic-elastic junction. The ratio of the covered plastic deformed wall thickness portion to the total wall thickness gives the autofrettage degree (Basara,2007)

$$A_d = \frac{r_j - r_{in}}{r_{out} - r_{in}} \cdot \%100 \quad (4.2)$$

Initial yielding of the material at the inner surface of an elastic thick-walled tube will start when the internal pressure achieves,

$$P_{in,rin}^{Closed\ end} \leq \frac{Re}{\sqrt{3}} \left[ 1 - \frac{r_{in}^2}{r_{out}^2} \right] \quad (4.3)$$

For closed end conditions  $\sigma_z \neq 0$ , Equation 4.4 is used (Maximum distortion strain energy criteria)

$$\sigma_e = \sqrt{0.5 [(\sigma_\varphi - \sigma_z)^2 - (\sigma_z - \sigma_r)^2 - (\sigma_r - \sigma_\varphi)^2]} = \sqrt{3} p_{in, rin} \cdot \frac{\left(\frac{r_{out}}{r}\right)^2}{\left(\frac{r_{out}}{r_{in}}\right)^2 - 1} \Big|_{r=r_{in}} \leq Re \quad (4.4)$$

$$P_{in, rin}^{opened\ end} \leq \frac{Re}{\sqrt{3}} \left[ 1 - \frac{r_{in}^2}{r_{out}^2} \right] \cdot \left| 1 + \frac{r_{in}^4}{3 \cdot r_{out}^4} \right|^{-1/2} \quad (4.5)$$

For open end conditions  $\sigma_z = 0$

The magnitude of the internal pressure which causes yielding of a tube with closed ends up to a radius  $r_j$  can be determined from a boundary condition whereby the magnitude of the radial stress component at the inner surface is equal to the negative magnitude of the internal pressure.

#### 4.2.1.1 Stress Distribution in a Partially Autofrettaged Tube

By applying the boundary conditions that the radial stress component at the outer surface of a tube is zero and that a tube yields up to the elastic-plastic junction where the distortional energy density Equation 4.4 reaches a value equal to the distortional energy density at yield in an uniaxial case,  $(\sigma_r - \sigma_z) \leq \frac{2 \cdot Re}{\sqrt{3}}$  can be solved with  $(\sigma_\varphi - \sigma_r - r \cdot \frac{d\sigma_r}{dr} = 0)$ . The solution gives expressions for the tangential and radial stress components within the elastic region of a partially autofrettaged thick-walled tube.

Therefore, general expressions for the distribution of stresses across the elastic region (er) of a partially autofrettaged thick-walled tube (Pa) are given by (Basara, 2007)

$$\sigma_{\varphi,pa,er} = \frac{Re}{\sqrt{3}} \cdot \left| \frac{r_j^2}{r_{out}^2} + \frac{r_j^2}{r^2} \right| - \left[ \Delta p \cdot \frac{\left(\frac{r_{out}}{r}\right)^2 + 1}{\left(\frac{r_{out}}{r_{in}}\right)^2 - 1} \right] \quad (4.6)$$

$$\sigma_r,pa,er = \frac{Re}{\sqrt{3}} \cdot \left| \frac{r_j^2}{r_{out}^2} - \frac{r_j^2}{r^2} \right| + \left[ \Delta p \cdot \frac{\left(\frac{r_{out}}{r}\right)^2 - 1}{\left(\frac{r_{out}}{r_{in}}\right)^2 - 1} \right] \quad (4.7)$$

$$\sigma_z,pa,er = \frac{Re}{\sqrt{3}} \cdot \frac{r_j^2}{r_{out}^2} - \left[ \Delta p \cdot \frac{1}{\left(\frac{r_{out}}{r_{in}}\right)^2 - 1} \right] \quad (4.8)$$

Where  $\Delta p = P_{in,rj} - P_{in}$  is the pressure difference between the autofrettage pressure, which causes yielding of a tube up to the radius  $r_j$  and actual applied internal pressure ( $p_{in}$ ).

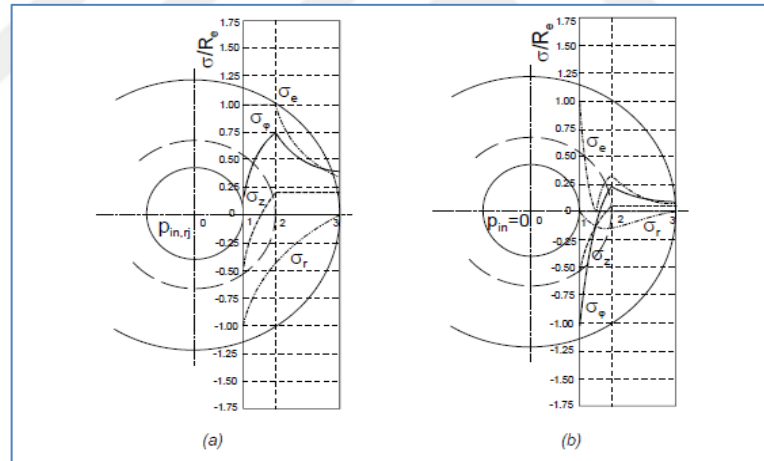


Figure 4.5. a) Distribution of applied principal stresses across the wall of a partially autofrettaged tube subjected to the internal pressure ( $P_{in,rj}$ ) b) Distribution of residual principal stresses across the wall of a partially autofrettaged tube unloaded to a zero pressure.

General expressions for the distribution of stresses across the plastic region ( $p_r$ ) of a partially autofrettaged thick-walled tube (Pa) are given by Figure 4.5



$$\sigma_{\varphi,pa,pr} = \frac{Re}{\sqrt{3}} \cdot \left| 1 + \frac{r_j^2}{r_{out}^2} - 2 \cdot \ln \frac{r_j}{r} \right| - \left[ \Delta p \cdot \frac{\left(\frac{r_{out}}{r}\right)^2 + 1}{\left(\frac{r_{out}}{r_{in}}\right)^2 - 1} \right] \quad (4.9)$$

$$\sigma_{r,pa,pr} = -\frac{Re}{\sqrt{3}} \cdot \left| 1 - \frac{r_j^2}{r_{out}^2} + 2 \cdot \ln \frac{r_j}{r} \right| + \left[ \Delta p \cdot \frac{\frac{r_{out}^2}{r} - 1}{\left(\frac{r_{in}}{r}\right)^2 - 1} \right] \quad (4.10)$$

$$\sigma_{z,pa,pr} = \frac{Re}{\sqrt{3}} \cdot \left[ \frac{r_j^2}{r_{out}^2} - 2 \cdot \ln \frac{r_j}{r} \right] - \left[ \Delta p \cdot \frac{1}{\left(\frac{r_{out}}{r_{in}}\right)^2 - 1} \right] \quad (4.11)$$

Where  $\Delta p = \mathbf{P}_{in,rj} - \mathbf{P}_{in}$  is the pressure difference between the autofrettage pressure ( $\mathbf{P}_{in,rj}$ ) which causes the yielding of the tube up to the radius  $r_j$  and the actual applied pressure. If the tube is unloaded and afterwards repressurized with internal pressure  $0 \leq \mathbf{P}_{in} \leq \mathbf{P}_{in,rj}$ , the state of the total principal stresses in the plastic region could be expressed by Equations 4.9 to 4.11.

#### 4.2.1.2 Strain Distribution in a Partially Autofrettaged Tube

Figure 4.12 shows strain distribution in a partially autofrettage tube.

$$\varepsilon_{\varphi,pr}^t = \frac{1}{E} \cdot [\sigma_{\varphi} - 0.5(\sigma_r + \sigma_z)] + \frac{1}{\nu} \cdot [\sigma_{\varphi} - 0.5(\sigma_r + \sigma_z)] = \frac{1}{T} \cdot [\sigma_{\varphi} - 0.5(\sigma_r + \sigma_z)] \quad (4.12)$$

$$\varepsilon_{r,pr}^t = \frac{1}{E} \cdot [\sigma_r - 0.5(\sigma_{\varphi} + \sigma_z)] + \frac{1}{\nu} \cdot [\sigma_r - 0.5(\sigma_{\varphi} + \sigma_z)] = \frac{1}{T} \cdot [\sigma_r - 0.5(\sigma_{\varphi} + \sigma_z)] \quad (4.13)$$

$$\varepsilon_{z,pr}^t = \frac{1}{E} \cdot [\sigma_z - 0.5(\sigma_{\varphi} + \sigma_r)] + \frac{1}{\nu} \cdot [\sigma_z - 0.5(\sigma_{\varphi} + \sigma_r)] = \frac{1}{T} \cdot [\sigma_z - 0.5(\sigma_{\varphi} + \sigma_r)] \quad (4.14)$$

Where P is the slope of the true stress-plastic strain curve ( plastic modulus), E is the slope of the true stress-elastic strain curve (modulus of elasticity), T is the slope of the true stress-strain curve including the elastic strain (tangent modulus), the relationship between them being  $(1/T) = (1/E) + (1/P)$  (Basara, 2007).

#### 4.2.1.3. Residual Stress Pattern

Stresses that remain after the original cause of the stresses (external forces, eat gradient) have been removed, are called the residual stresses. When an internal pressure (Autofrettage Pressure) is applied to the cylinder, the wall becomes plastic up to a certain portion of the cylinder. When the autofrettage pressure is released, there is some compressive stress left in the cylinder due to elasto-plasticity. This compressive stress reduces maximum von Mises stress when another pressure known as the working pressure is applied and hence increases the capacity of the cylinder.

Ghomi and Majzoobi proposed a set of equations for different regions of the autofrettaged cylinder to calculate residual, radial and hoop stresses. From these equations, the residual stress patterns shown in Figure 4.5 are obtained ( Amin, Rayhan & Ahmed, 2013).

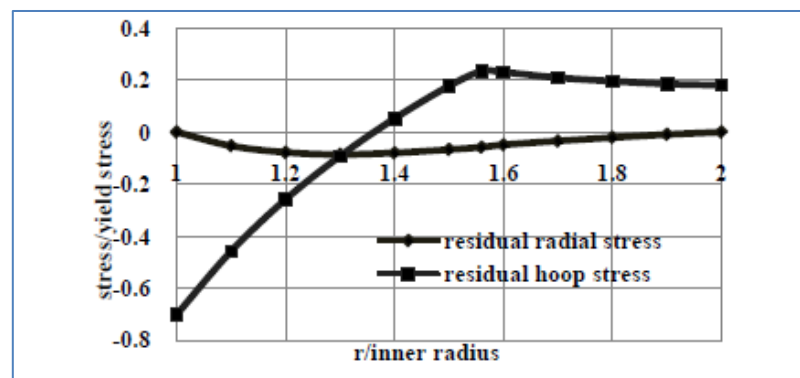


Figure 4.6 Residual stress pattern in autofrettaged cylinder.

From Figure 4.6, it is observed that the residual compressive hoop stress occurs near the bore and the residual radial stress occurs in the outer bore region.

#### 4.2.1.4 Optimum Radius of Elasto-Plastic Junction

From Figure 4.6 it is observed that when the working pressure is applied to the cylinder, the maximum von Mises stress decreases as the radius of elasto-plastic junction increases. It decreases to a certain value and then again starts to increase. The point where the maximum von Mises stress is minimum, is the optimum radius of the elasto-plastic junction (Amin, Rayhan & Ahmed, 2013).

a) Based on strength theory ( Tresca-yield ) (4.15)

$$r_{opt} = a \exp ( p_w / \sigma_y )$$

b) Based on strength theory ( von Mises ) (4.16)

$$r_{opt} = a \exp ( \sqrt{3} p_w / 2 \sigma_y )$$

Strength theory has been used to calculate  $r_{opt}$  from Figure 4.6 ( Amin, Rayhan & Ahmed, 2013).

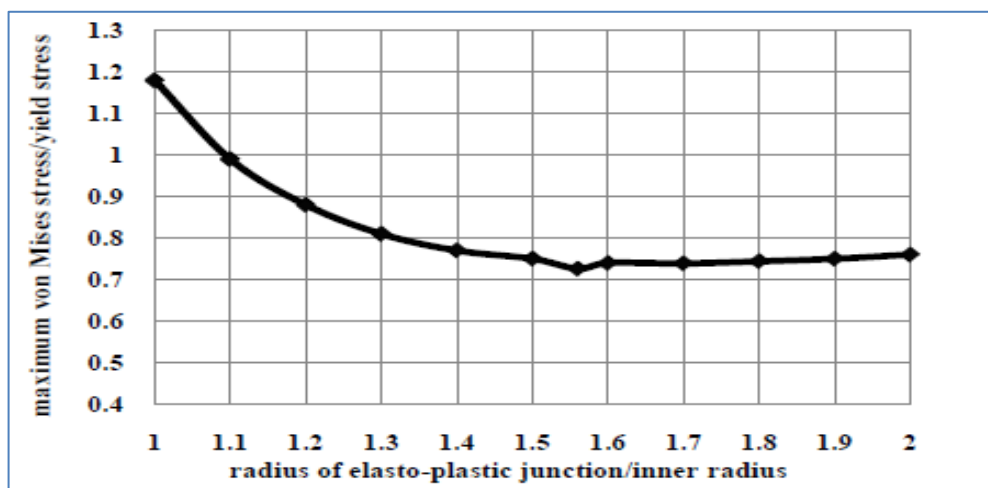


Figure 4.7 Variation of maximum von Mises stresses at different elasto-plastic radius.

To observe the effect of  $k$  on optimum radius of elastic-plastic junction Figure 4.7 is considered.

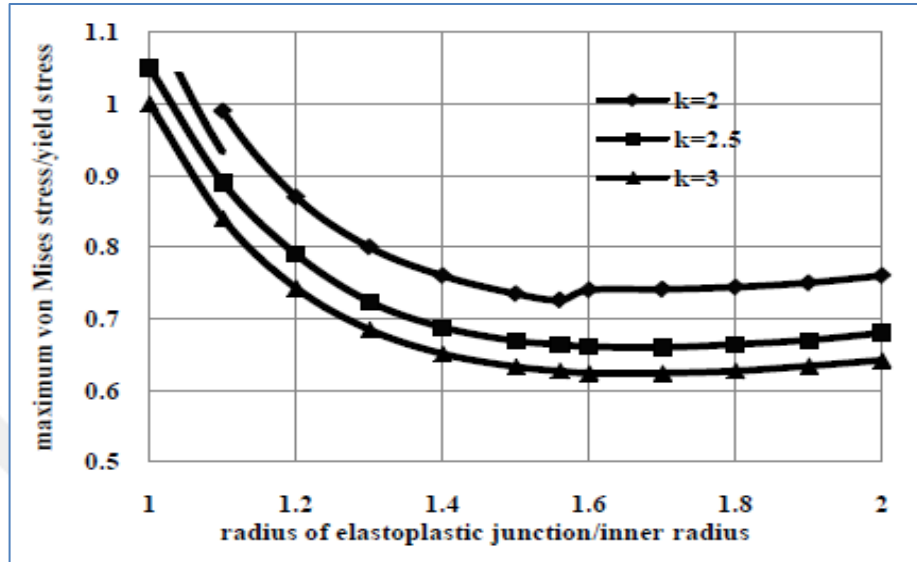


Figure 4.8 Variation of maximum von Mises stresses at different elasto-plastic radii for different  $k$  values.

It is observed that the values of  $r_{opt}$  are not the same for different values of  $k$  though  $p_w$  and  $\sigma_y$  are constant. As the values of  $k$  increases,  $r_{opt}$  tends to be increased. In the basis of material properties and  $k$  (outer radius / inner radius) the two pressure limits of autofrettage process are, (Amin, Rayhan & Ahmed, 2013).

$$P_{y1} = \sigma_y \frac{\left(1 - \frac{1}{k^2}\right)}{\sqrt{3}} \quad (4.17)$$

$$P_{y2} = \sigma_y \ln(k) \quad (4.18)$$

Where,  $P_{y1}$  is the pressure at which yielding starts at inner surface and  $P_{y2}$  is the pressure at which plasticity spreads throughout the cylinder. That means autofrettage effect will start at  $P_{y1}$  and continue affecting up to  $P_{y2}$ . Before  $P_{y1}$ , there will be no autofrettage effect as any portion of the cylinder does not go to plastic regime, hence

flow stress distribution throughout the thickness remains unchanged. After  $P_{y2}$ , there will be an adverse effect and capacity of the cylinder will decrease.

Assumptions show that, there is always significant deviation between simulations and equations ( Amin, Rayhan & Ahmed, 2013).

#### 4.2.1.5 Effect of Working Pressure

In Figure 4.8, it is observed that at first the maximum von Mises stress (MVS) decreases as autofrettage pressure increases. Maximum von Mises decreases up to a certain minimum value. After that MVS starts to increase again. This minimum value gives the optimum point. Figure 4.9 shows that, the autofrettage pressure corresponds to which the maximum von Mises stress is minimum, is the optimum autofrettage pressure,  $P_{opt}$ .

$$P_{opt} = \frac{\sigma_y}{2 \left[ 1 - \left( 1 - 2p/\sigma_y \right) \exp\left(\frac{2p}{\sigma_y}\right) \right]} + p \quad (\text{Tresca-yield}) \quad (4.19)$$

$$P_{opt} = \frac{\sigma_y}{3 \left[ 1 - \frac{\sqrt{3}p}{\sigma_y} \exp\left(\frac{\sqrt{3}p}{\sigma_y}\right) \right]} + p \quad (\text{von Mises}) \quad (4.20)$$

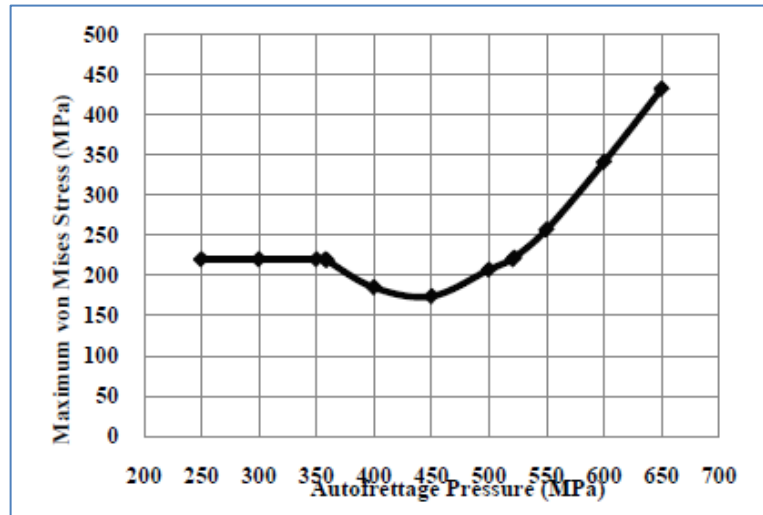


Figure 4.9 Variation of maximum von Mises stresses at different autofrettage pressure.

P is the working pressure in Equations 4.19 and 4.20. The comparison with Zhu & Yang's  $P_{opt}$  based on fourth strength theory. However autofrettage parameter is a very critical parameter for rail design, the gun drill diameter, micro-hole diameter and location of the micro-hole are other important factors. FEA results and test comparison will be evaluated in next pages.

**CHAPTER FIVE**  
**NUMERICAL RESULTS AND SIMULATIONS**

**5.1 Modelling**

For numerical simulations and modelling ANSYS 15.1 has been used. It has the elastic-plastic material modelling. Design studies have been made by ANSYS 15.1 Workbench Design Modeller. The material properties and geometric features of steel are summarized in Tables 5.1 and 5.2.

Table 5.1 Mechanical properties of steel for FEA inputs

<b>Material</b>	<b>Yield Strength (MPa)</b>	<b>Elasticity Modules (MPa)</b>	<b>Poisson Ratio</b>	<b>Ultimate Strength (MPa)</b>	<b>Tangent Modules (MPa)</b>
Micro-alloy steel	680	$2.1 \times 10^5$	0.3	1100	32023

Table 5.2 Geometric features of cylinder

<b>Working Pressure (bar)</b>	<b>Internal radius (a) mm</b>	<b>External Radius (b) mm</b>	<b>Radius ratio (k)</b>
<b>2000</b>	<b>4.5</b>	<b>11</b>	<b>2.44</b>

A single steel cylinder of internal radius a: 9 mm and b: 22 mm is considered. Figure 5.1 shows the inner and outer diameter of the rail tube.

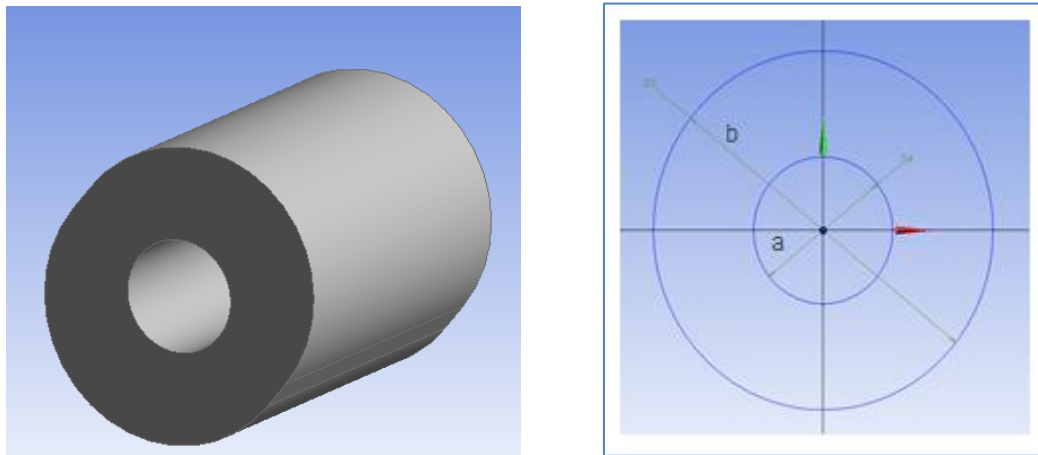


Figure 5.1 Section of tube.

## 5.2 Theoretical Calculation

Optimum elastic-plastic radius ( $r_{opt}$ ) is one of the most important design parameters and can be calculated on the basis of working pressure, yield strength and outer radius / inner radius ( $k$ ).

Based on von Mises criteria, (Equations 4.15 – 4.16 – 4.17 – 4.18)

$$r_{opt} : 1.29 \text{ mm}$$

$$P_{y1} : 326.65 \text{ MPa} = 3260 \text{ Bar}$$

$$P_{y2} : 606.65 \text{ MPa} = 6065 \text{ Bar}$$

Analytical calculations show that, for the considered cylinder (22x9 – Circular)  $P_{y1}$  is 3260 Bar and  $P_{y2}$  is 6065 Bar. This shows that autofrettage will start at 3260 Bar and continue affecting up to 6065 Bar. Before 3260 Bar there will no autofrettage effect as any portion of the cylinder does not go to plastic regime, thus flow stress distribution in the cylinder remains unchanged. After 6065 Bar there will be an adverse effect and capacity of the cylinder will decrease. This adverse effect can happen during burst tests. Crack could be observed in the rail tube. Optimum elastic-plastic radius ( $r_{opt}$ ) is calculated as  $r_{opt} : 1.29 \text{ mm}$ .



Table 5.3 Analytic results of the rail tube

<b>Geometry (k)</b>	<b><math>r_{opt}</math></b>	<b><math>P_{y1}</math></b>	<b><math>P_{y2}</math></b>
22/9 = 2.44	1.29	3260	6065

For numerical simulations, FEA analysis will be carried out. **7000** Bar AF pressure will be applied. Optimum elastic-plastic radius will be determined in next pages.

### 5.3 FEA Analysis

#### 5.3.1 Meshing

22X9 (Circular Design) has been modelled by ANSYS 15.1 in design modeller module. Here the design goal is to identify the stress distribution along bore diameter. Figure 5.2 shows the mesh detail of the bore. The inner diameter and cutted section were meshed separately, which were mapped by face meshing style.

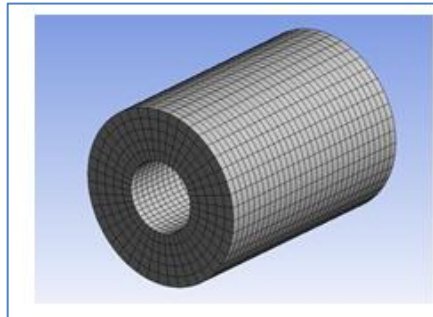


Figure 5.2 Schematic of meshing.

#### 5.3.2 Boundary Conditions and Loading

Figure 5.3 shows the loadings and boundary conditions. Frictionless support was used for cut surfaces. System pressure is applied to the inner bore of the tube.

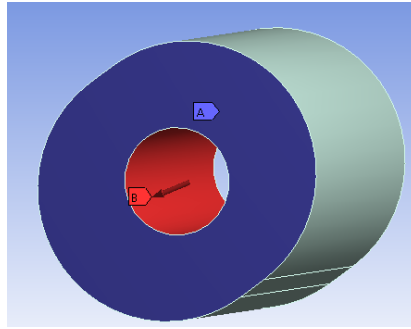


Figure 5.3 Boundary conditions and loading.

### 5.3.3 Analysis Settings

Two kinds of analyses are represented to determine the autofrettage effect on the product design. A Path is created to see the stress distribution along the section, Figure 5.4.



Figure 5.4 Path section.

There is no autofrettage effect in 1st analysis. Analysis is implemented at three load steps. During the analysis only the system pressure (2000 bar) is applied. The load steps are given below,

1st Load step : Applied Running Pressure (2000 Bar)

2nd Load Step : Removed Running Pressure

3rd Load Step : Applied Running Pressure (2000 Bar)

Second analysis is implemented at five load steps. Autofrettage effect was represented.

1st Load Step : Applied Autofrettage Pressure (7000 Bar)

2nd Load Step : Removed Autofrettage Pressure

3rd Load Step : Applied Running Pressure (2000 Bar)

4th Load Step : Removed Running Pressure

5th Load Step : Applied Running Pressure (2000 Bar)

### 5.3.3.1 Results of First Analysis

Linear elasticity modelling is used for the rail tube. No autofrettage pressure is applied. Figure 5.5a shows the loading applied at FEA analysis. Figure 5.5b shows the stress distributions on the cylinder.

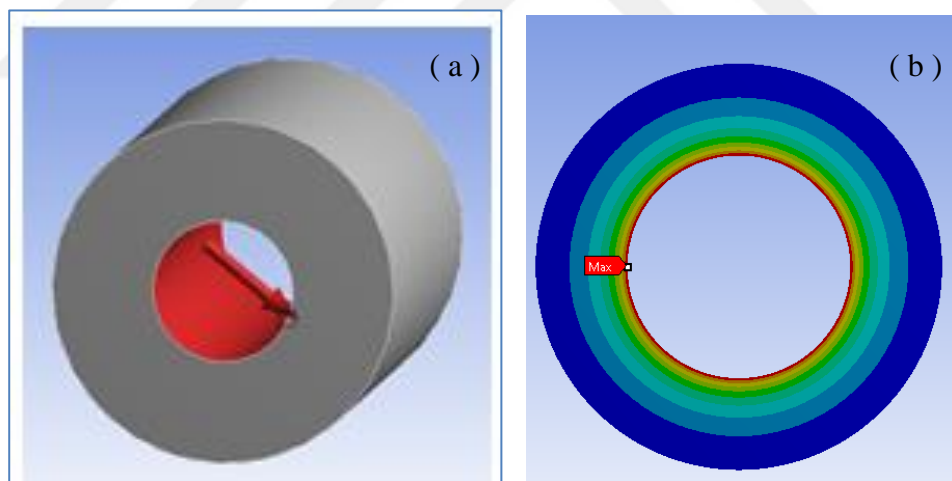


Figure 5.5 a) Schematic of pressure loading, b) stress distribution on cylinder

On the cylinder, maximum principle stress occurs in the inner bore. The maximum stress value is obtained as 279.14 MPa. The minimum principle stress occurs at the inside of the outer bore. This stress value is -198.74 MPa.

The maximum principle stress represents a tensile stress, whereas the minimum principle stress represents a compressive stress in simulation. Figure 5.6 shows stress distribution along the thickness.

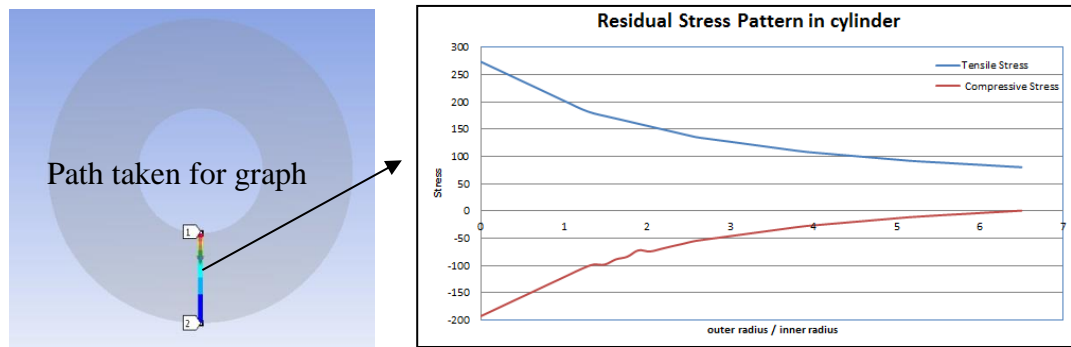


Figure 5.6 Stress distributions along cylinder thickness.

### 5.3.3.2 Results of 2nd Analysis

Bi-linear kinematic hardening model is used for the cylinder. Autofrettage pressure was carried out as 7000 bar. Autofrettage pressure was determined to examine the stress distributions throughout the cylinder, Figure 5.7.

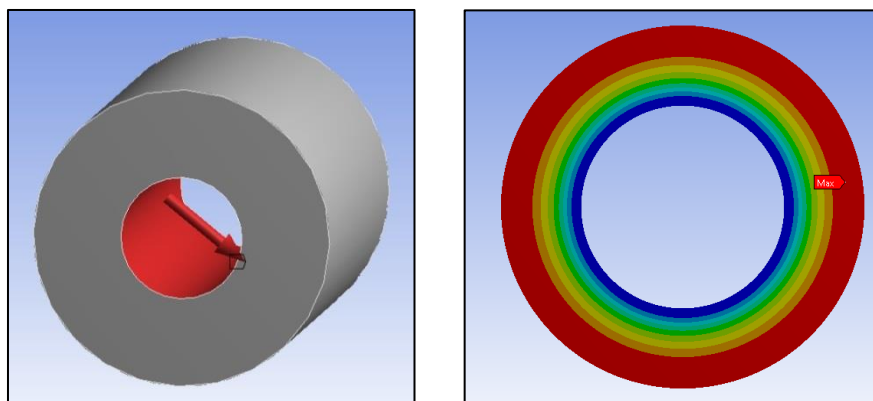


Figure 5.7 a) Schematic of pressure loading, b) stress range on cylinder.

In autofrettaged cylinder, maximum principle stress occurs on the sub-surface of the outer bore. This stress value is 436.83 MPa. The minimum principle stress occurs at the inner sub-surface. This value is -478.86 MPa. The maximum principle stress represents a tensile, and minimum principle stress represents a compressive stress in simulation. Figure 5.8 shows the stress distribution along the thickness.

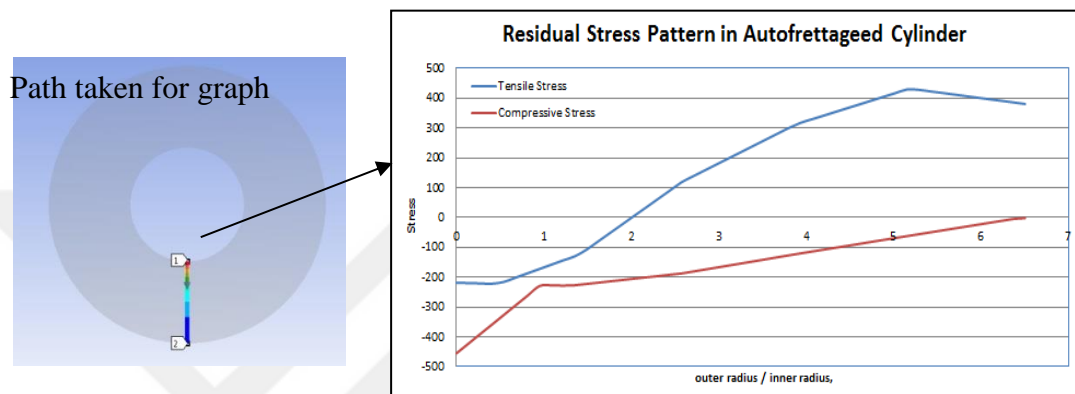


Figure 5.8 Stress distributions along cylinder thickness.

Table 5.4 Comparison of rail tube with autofrettage and without autofrettage

	<b>Tensile Stress ( MPa)</b>	<b>Compressive Stress (MPa)</b>
With Autofrettage	436.83	-478.86
Without Autofrettage	279.14	-198.174

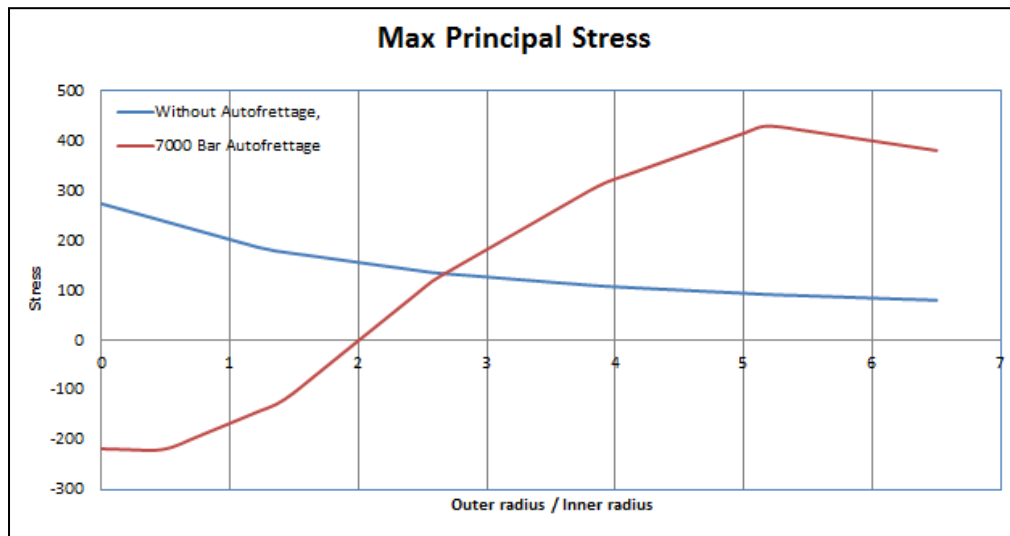


Figure 5.9 Comparison of stress distributions (with autofrettage and without autofrettage).

Figure 5.9 and Table 5.4 show that, autofrettage changes the stress location rather than the stress value in rail tube. Without autofrettage, the maximum stress is observed at the inner radius of rail tube. When autofrettage is applied the stress location changes throughout the outer radius.

By autofrettage, the maximum stress value does not decrease but location of the maximum stress changes. Without autofrettage the maximum stress occurs at the inner bore, during the operation of the system, this stress causes fatigue cracks. The fatigue life of component can be affected in a negative manner. Autofrettage generates compressive residual stress at the inner bore. This residual stress reduces von Mises stresses. When the autofrettage pressure is released, there is some compressive stress left in the cylinder due to elasto-plasticity. This compressive stress reduces the maximum von Mises stress when another pressure known as the working pressure is applied. Figure 5.9 shows that  $r_{opt}$  where maximum von Mises stress is minimum, is the optimum radius of elasto-plastic junction. Figure 5.10 shows that  $r_{opt}$  is 0.9472 mm. That means that the bore will be plastified until 0.9472 mm by autofrettage pressure. Autofrettage is a necessary design parameter for rail. Because without modifying the geometry, higher pressures could be achieved.

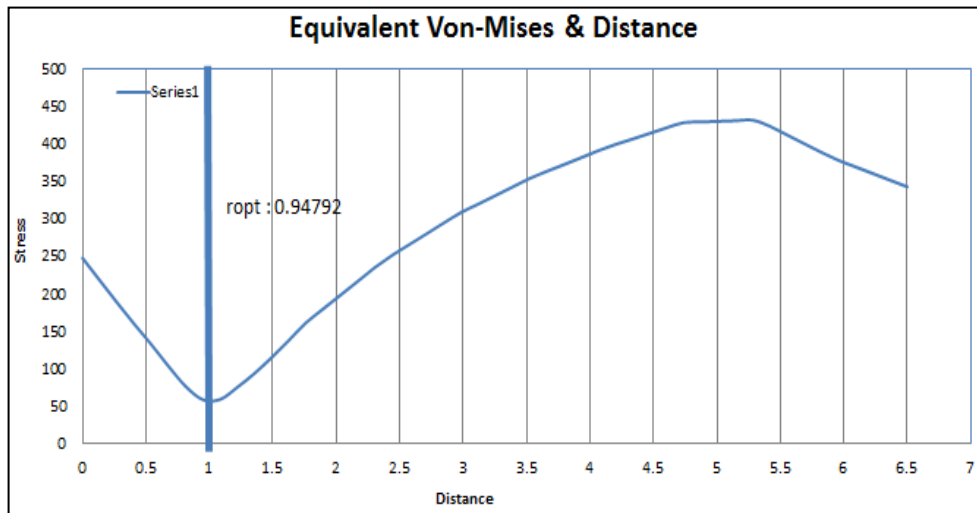


Figure 5.10 Comparison of elasto-plastic radius and minimum von Mises stress.

Table 5.5 ‘ $r_{opt}$ ’ value for analytical and simulation result

	AF Pressure	Analytical Approach	FEA Result
$r_{opt}$	7000 Bar	1.29mm	0.94792 mm

It is observed from Table 5.5 that there is always significant deviation between analytical results and FEA results.  $r_{opt}$  is related to the working pressure, yield strength, outer radius / inner radius more than the other design parameters.

### 5.3.4 Oblong Design

There are two different types of external shapes for the rail body. Figure 5.11a shows the oblong shape. The basic difference between the oblong and circular shapes is that the oblong shape is lighter than the circular shape. Also the oblong shape is longer than circular shape along the horizontal axis. FEA analysis will be carried out to show the difference between both designs.

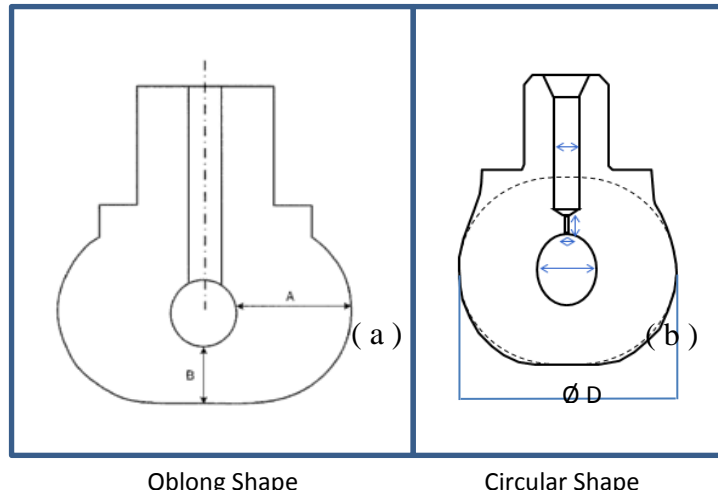


Figure 5.11 a) Oblong shape , b) Circular shape.

To avoid illogical results, same meshing settings, and same boundary conditions are applied during FEA study. The FEA in Figure 5.12 shows that autofrettage has a positive effect on the product. Thus autofrettage will be directly applied at next analysis. Bi-linear kinematic hardening modelling will be used.

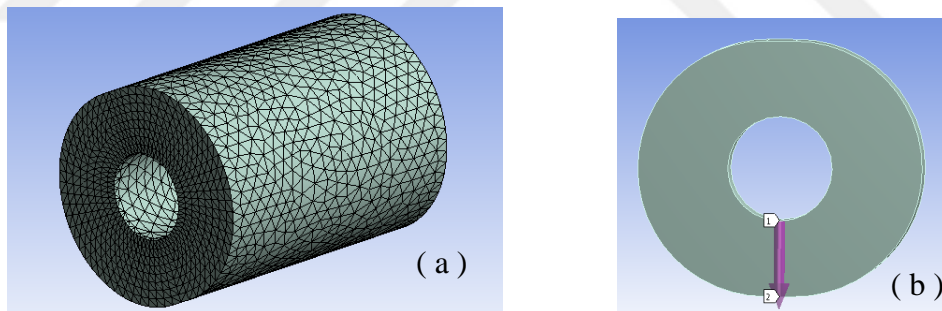


Figure 5.12 a) Meshing , b) Path definition.

Analysis was carried out at 7000 autofrettage Bar. Oblong design gives similar results compared with the circular design for the same autofrettage pressure. Both designs have the same  $r_{opt}$  value; however von Mises stresses are different. Figure 5.13 shows  $r_{opt}$  and minimum von Mises stress comparison.



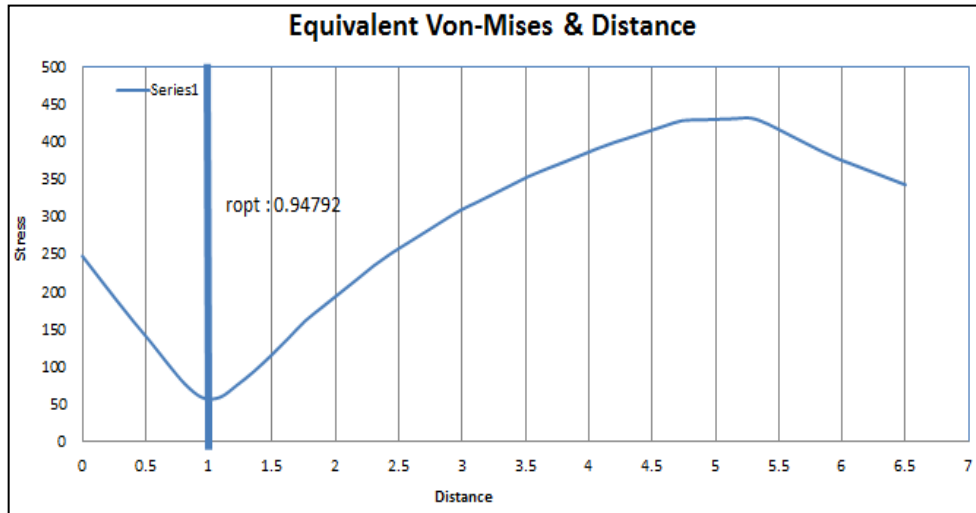


Figure 5.13 Comparison of elasto-plastic radius and minimum von Mises stress.

Table 5.6 Overall results for circular and oblong design

		MPA				mm
		Equivalent Stress ( von Mises)	Compressive Stress	Tensile Stress	Minimum Stress (von Mises )	$r_{opt}$
Circular		432.1	-487.64	436.83	51.229	0.94792
Oblong		431	-489.15	490	69.379	0.94792

Table 5.6 shows that,

- Both design show similar stress distribution. Stress values are very close.
- Circular design has minimum lower von Mises stress value than the oblong design for the same optimum elastic-plastic radius ( $r_{opt}$ ).
- Analytical and FEA results show similarity with very little deviation.
- Although results are similar, the micro-hole effect must be evaluated separately.

- The yield point, working pressure and rail tube diameter have major effects on the rail robustness during the operation of the system.
- Autofrettage pressure and  $r_{opt}$  are the major design parameters of the rail. These parameters are related to the working pressure, yield strength,  $k$  (outer radius / inner radius) more than the other effects.

### 5.3.5 FEA Results for Micro- Hole Design

When the rail geometry is examined, it is seen that the weakest area is the high pressure outlet section. The micro-hole calibrates the fuel before the injector. During the operation of the system, micro-hole undergoes cyclic loadings between maximum and minimum pressures. Since the micro-hole section is critical, the FEA simulation needs to be carried out.

#### 5.3.5.1 Oblong Design

- Micro-hole section has been modeled as seen in Figure 5.14a
- Micro-hole section is meshed separately to obtain more accurate results as seen in Figure 5.14b
- The same boundary conditions and loadings are applied
- 7000 Bar autofrettage pressure is applied
- LS3 is based on observing the autofrettage effect on micro-hole

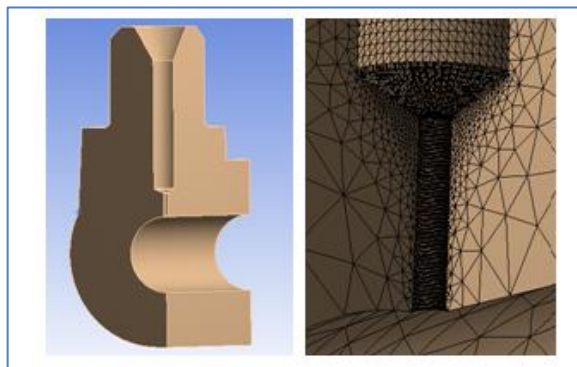


Figure 5.14. a) Micro-hole design b) Micro-hole meshing.

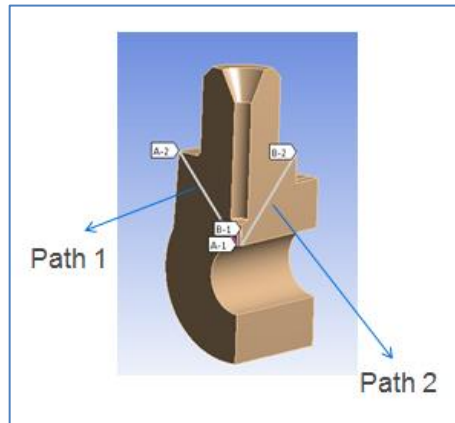


Figure 5.15 Path for micro-hole design.

### 5.3.5.2 Circular Design

- Micro-hole section has been modeled as shown in Figure 5.17a
- Micro-hole section is meshed separately to obtain more accurate results as seen in Figure 5.17b
- Same boundary conditions and loadings are applied
- 7000 Bar autofrettage pressure is applied
- LS3 is based on observing the autofrettage effect on micro-hole

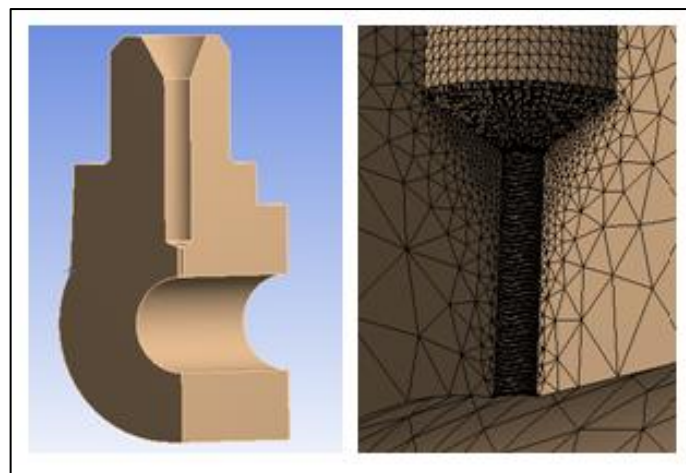


Figure 5.16 a) Micro-hole design b) Micro-hole meshing.

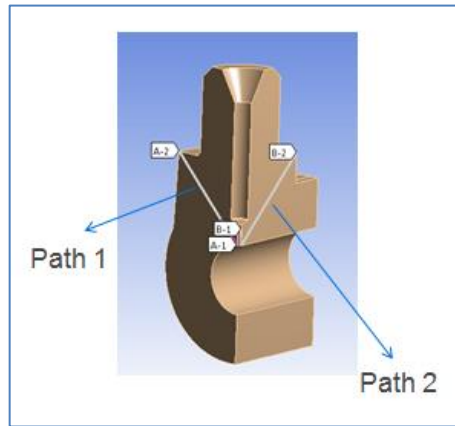


Figure 5.17 Path for micro-hole design.

Paths are created to see stress distributions. As shown in Figure 5.18, path 1 represents the radial stress distribution and path 2 represents axial stress distribution.

## CHAPTER SIX RESULTS

Figures 6.1 and 6.2 show overall compressive stress and tensile stress distributions of the rail section. Micro-hole designs show similarity, however stress values are different from each other. Designs with and without micro-holes show similar distributions.

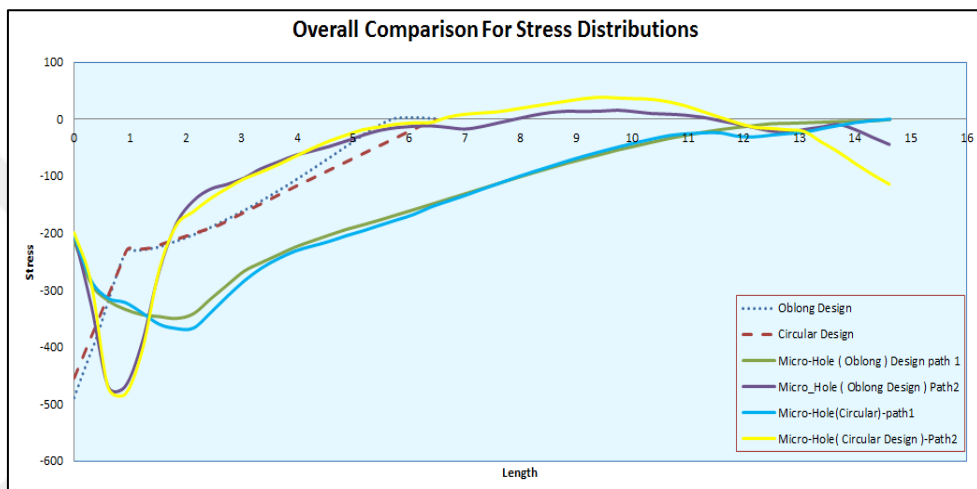


Figure 6.1 Overall comparisons of compressive stress distributions.

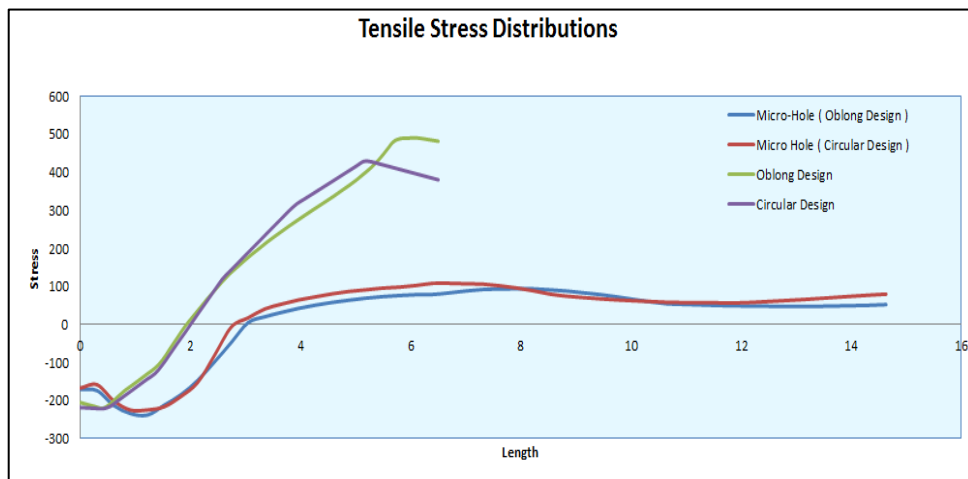


Figure 6.2 Overall comparisons of tensile stress distributions.

Results can be summarized at two steps,

- Step 1 Oblong – Circular comparison (without micro-hole)
- Step 2 Oblong – Circular Comparison (with micro-hole)

Table 6.1 Overall results

	Without Micro- Hole		Oblong ( Micro- Hole )		Circular ( Micro –Hole )	
	Circular	Oblong	Path 1	Path 2	Path 1	Path 2
Von –Mises Stress ( MPa)	432.11	431	243.93	440.81	293	470
Minimum Von – Mises Stress ( MPa)	59.229	69.379	NA	NA	NA	NA
Compressive Stress ( MPa )	-487.64	-489.15	-34.89	-469.3	-367	-483
Tensile Stress ( MPa )	436.83	490	94.105	485.21	108	542
$R_{opt}$ ( mm )	0.94792	0.94792	NA	NA	NA	NA

### 6.1 Step 1 (Oblong–Circular comparison Without Micro– hole)

Regarding Tables 6.1 and 6.2, both designs have similar stress values. Circular design is has negligibly better stress values than the oblong design.  $r_{opt}$  which is one of the most important design parameters for the rail tube is the same for both designs, since both design has the same yield strength and working pressure.  $P_{y1}$  and  $P_{y2}$  (autofrettage start pressure and autofrettage end pressure) are the same for both designs.  $P_{y1} = 3260$  bar and  $P_{y2} = 6065$  Bar (analytical calculations). 7000 Bar is used as FEA parameter as used on serial production. The only difference between these calculations is that analytical calculations were made for the tube design.

Table 6.2 Comparison of FEA results and analytical calculation

	<b>Geometry (k)</b>	<b>R<sub>opt</sub></b>	<b>P<sub>y1</sub></b>	<b>P<sub>y2</sub></b>
Analytical Calculation	11/4.5 =2.44	1.29 mm	3260 MPa	6065 MPa
FEA results	11/4.5=2.44	0.94792	7000 (FEA input)	7000 (FEA input)

### 6.2 Step 2 (Oblong–Circular comparison With Micro– hole)

First of all, it's very hard to define  $r_{opt}$  from von Mises stress graphics. Due to micro–hole geometry, minimum stress range changes at many places. Thus analytical and FEA results cannot be compared. And also all previous analytical studies have been conducted for cylinder geometry. Oblong design obtains lower stress values than the circular design.

Table 6.3 Difference in stress values

	<b>Oblong (Micro-Hole)</b>		<b>Circular (Micro-Hole)</b>		<b>Difference (MPa)</b>	
	Path1	Path2	Path1	Path2	Path1	Path2
von Mises	243.93	440.81	293	470	49.07	29.19
Compressive	-349.89	-469.63	-367	-483	18	14
Tensile	94.105	485.21	108	542	15	57

Due to Table 6.3 oblong design has lower stress values than the circular design. At the same time, oblong design is lighter than the circular design. Analytical approach cannot be used for micro-hole studies. Due to micro-hole geometry, stress location changes and  $r_{opt}$  cannot be defined, thus minimum von Mises value cannot be clarified.

## CHAPTER SEVEN

### CONCLUSIONS

In this study design parameters of rail tube are defined in basis of analytical and FEA simulations and the two analyses were compared with each other. FEA results and calculations show that autofrettage is one of the most important design parameters of the rail tube. Autofrettage pressure and the optimum elastic-plastic radius are other items of the autofrettage process. Except from autofrettage, outer shape of the rail is another design parameter. FEA results show that the oblong design has lower stress values compared to the circular design. All of the results of these studies must be verified by testing methodology such as fatigue tests.

The following conclusions have been obtained as a result of this study;

- 1- Optimum elastic-plastic radius is related with the working pressure, yield strength and outer radius / inner radius.
- 2- As far as the working pressure increases, autofrettage pressure also increases.
- 3- Optimum elastic-plastic radii occur where the von Mises stress is minimum.
- 4- Although stress values are close to each other, oblong design is preferred because of its lightweight.
- 5- Autofrettage pressure must be higher than the working pressure, hence the material can be plastified.
- 6- There are significant deviations between analytical calculations and FEA simulations. Thus these values must be correlated by fatigue testes.



## REFERENCES

- Aktekin, N. (2013). *Delphi product training*. Delphi Dizel Otomotiv Ticaret Limited Şirketi, İzmir.
- Amin, T., Rayhan, A., Ali, Tousif , A.A, & Faisal, A.A. (2013). *Optimum design of autofrettaged thick walled cylinder*. University of Engineering and Technology, Bangladesh.
- Basara, A.(2007). *Evaluation of high pressure components of fuel injection systems using speckle interferometry*. Germany : Shaker Verlag GmbH,
- Bosch, R. (2007). *Automotive handbook* (7<sup>th</sup> Ed). Germany: Robert Bosch GmbH.
- Gibson, C.M. (2008). *Determination of residual stress distribution in autofrettaged tubing*. PhD Thesis, Defence College of Management and Technology Cranfield University, England.
- Heywood, J. B. (1988). *Internal combustion engine fundamentals*. USA : McGraw-Hill Education
- Perry, J. & Aboudi, J. (2003). *Elasto-Plastic Stresses in Thick Walled Cylinder* Department of Solid Mechanics, Materials & Systems, Tel Aviv University, Israel, 125, 248-252.
- Villian, J.M. (2008). *Delphi material specification*. Delphi Dizel Otomotiv Ticaret Limited Şirketi, İzmir.
- Wahi, N., Ayob, A. & Elbasheer, K. M. (2011). Effect of autofrettage allowable pressure of thick-walled cylinders. 2011 *International Conference on Environmental and Agriculture Engineering*, Singapore

## APPENDICES

$r_{opt}$	(mm)	Optimum elastic-plastic radius
$P_{y1}$	(Bar)	Pressure which Autofrettage Start
$P_{y2}$	(Bar)	Pressure which Autofrettage End
$k$		Outer radius / inner radius
$P_{in}$	(Bar)	Internal Pressure
$P_{in,rin}$	(Bar)	Magnitude of internal pressure which causes yielding of material inner surface
$P_{in,rout}$	(Bar)	Magnitude of internal pressure required to bring complete wall of tube into a state plastic deformation
$P_{in,rj}$	(Bar)	Magnitude of internal pressure which causes yielding of tube out diameter
$\Delta P$	(Bar)	Pressure Difference
$T$	(N/mm <sup>2</sup> )	Tangent Modules
$E$	(N/mm <sup>2</sup> )	Modulus of Elasticity
$\sigma_y$	(N/mm <sup>2</sup> )	Yield Strength
$\sigma_{UTS}$	(N/mm <sup>2</sup> )	Tensile Strength
Max	-	Maximum value
Min	-	Minimum Value
Total	-	Total Value
$\varphi z$	-	$\varphi z$ Plane

t	-	Total component
e	-	Elongation
el	-	Elastic
er	-	Elastic Region

